Petrogenesis and tectonic significance of Neoproterozoic intrusions in Jebel Ja'alan, East Oman

Thesis submitted in accordance with the requirements of the University of Adelaide for an Honours Degree in Geology

George Gray Fleming Murray

November 2015

THE UNIVERSITY
of ADELAIDE

PETROGENESIS AND TECTONIC SIGNIFICANCE OF NEOPROTEROZOIC INTRUSIONS IN JEBEL JA'ALAN, EAST OMAN

IGNEOUS INTRUSIONS OF JEBEL JA'ALAN

ABSTRACT

Jebel Ja'lan, a basement inlier located in the east of the Sultanate of Oman, hosts an igneous intrusive suite. Oman lies to the south-east of the Arabian-Nubian Shield (ANS), which is a shield constructed mostly of amalgamated Neoproterozoic island arc terranes. This paper aims to calculate the age and tectonic setting of the Jebel Ja'alan intrusive suite and to understand its relationship to the ANS. The earliest intrusion of the field area, a granite batholith, is dated at ~840 Ma using U-Pb geochronology. The batholith is cross-cut by three petrologically distinct generations of dykes which have similar isotopic and geochemical signatures. All generations of the suite have positive εNd values between +0.56 to +6.78 and the granite returned positive εHf values of +2.30 to +10.17, suggesting a juvenile crustal origin. Rare earth element spider plots and tectonic classification diagrams provide evidence for an island arc setting of emplacement. Other studies of the Neoproterozoic intrusions of the ANS and the Oman basement show similar ages for island arc granite intrusions (850-830 Ma and ~845 Ma). Sm-Nd model ages of the dyke swarm of Jebel Ja'alan give Mesoproterozoic ages greater than the pre-dating granite which indicates contamination of the mantle wedge due to subduction. The dyke swarm has been interpreted from field studies and petrography to have an early stage of syn-collisional or post-tectonic emplacement, followed by a more pervasive anorogenic emplacement, possibly during extensional collapse. The Mirbat region and the arc terranes of Yemen and Sinai are cut by dyke swarms similar to Jebel Ja'alan that show island arc geochemistry and may all be coeval.

KEYWORDS

Petrogenesis; tectonics; Oman; Arabian-Nubian Shield; Gondwana; Neoproterozoic.

TABLE OF CONTENTS

LIST OF FIGURES AND TABLES

INTRODUCTION

The Arabian-Nubian Shield (ANS) forms part of the East African Orogen (EAO) (Meert 2003, Collins and Pisarevsky 2005). It is made up of several volcanic arc terranes bounded by ophiolites along suture zones (Johnson 2003, Cox et al. 2012). The EAO and ANS are shown in relation to the African continent and Arabia in Figure 1. To the east of the ANS is the Omani basement, which is thought to also be a series of arc terranes accreted during the closure of the Mozambique Ocean (Rantakokko et al. 2014). These terranes were likely to be close to or at the margin of Neoproterozoic India because of earlier cessation of accretion here compared to the ANS. The terranes were amalgamated due to India's subduction-related convergence towards the Saharan Craton (Rantakokko et al. 2014).

The Omani Basement is a poorly studied segment of Gondwana that could provide important clues to the timing of closure of the Mozambique Ocean, and ultimately, the amalgamation of Gondwana. At present the Jebel Ja'alan basement has not been studied for purposes of reconstructing Gondwana, but the Mirbat region in the south of Oman has seen some study in this area (Mercolli et al. 2006, Rantakokko et al. 2014, Gass et al. 1990, Worthing 2005). Mirbat contains the largest outcrop of Neoproterozoic rock in the country and it has been interpreted to be a volcanic arc terrane (Rantakokko et al. 2014). The Neoproterozoic rocks of Oman may also be important for providing evidence on the style of Gondwana amalgamation. As Gondwana geology has been more greatly studied, models of its amalgamation have developed from simple collisions between large continental masses to long-lived, multi-stage collisions between many terranes differing in size and origin (Collins and Pisarevsky 2005,

Johnson et al. 2011). The ANS itself is a powerful piece of evidence for multi-stage collisions as it is purported to have been accreted through the collision of multiple island-arc terranes (Meert and Lieberman 2007, Meert 2003, Meert and Van Der Voo 1997, Collins and Pisarevsky 2005, Rogers et al. 1995).

This paper hypothesises that the igneous intrusions of Jebel Ja'alan, Sultanate of Oman were emplaced as a result of subduction of oceanic crust as Gondwana came together in the Tonian. It is therefore, by extension, hypothesising that these Neoproterozoic rocks were emplaced much in the same manner as in the arc terranes of the ANS in Saudi Arabia (Robinson et al. 2014, Cox et al. 2012, Johnson et al. 2011) and the Mirbat Region (Rantakokko et al. 2014, Worthing 2005).

We aim to constrain the ages of each intrusion generation by obtaining U-Pb zircon dates, Lu-Hf zircon model ages, and Sm-Nd model ages from samples collected in the field area. This will provide an estimate of the time of melt partitioning and magma crystallization and thus help to constrain the timing of arc magmatism and any post-orogenic magmatism. We also aim to determine the tectonic setting that caused the emplacement of each intrusion by obtaining geochemical data from the samples. Different tectonic settings have unique geochemical signatures in their igneous rocks and by carrying out geochemical sampling we can determine whether each intrusive body in the Jebel Ja'alan was emplaced during arc or rift activity.
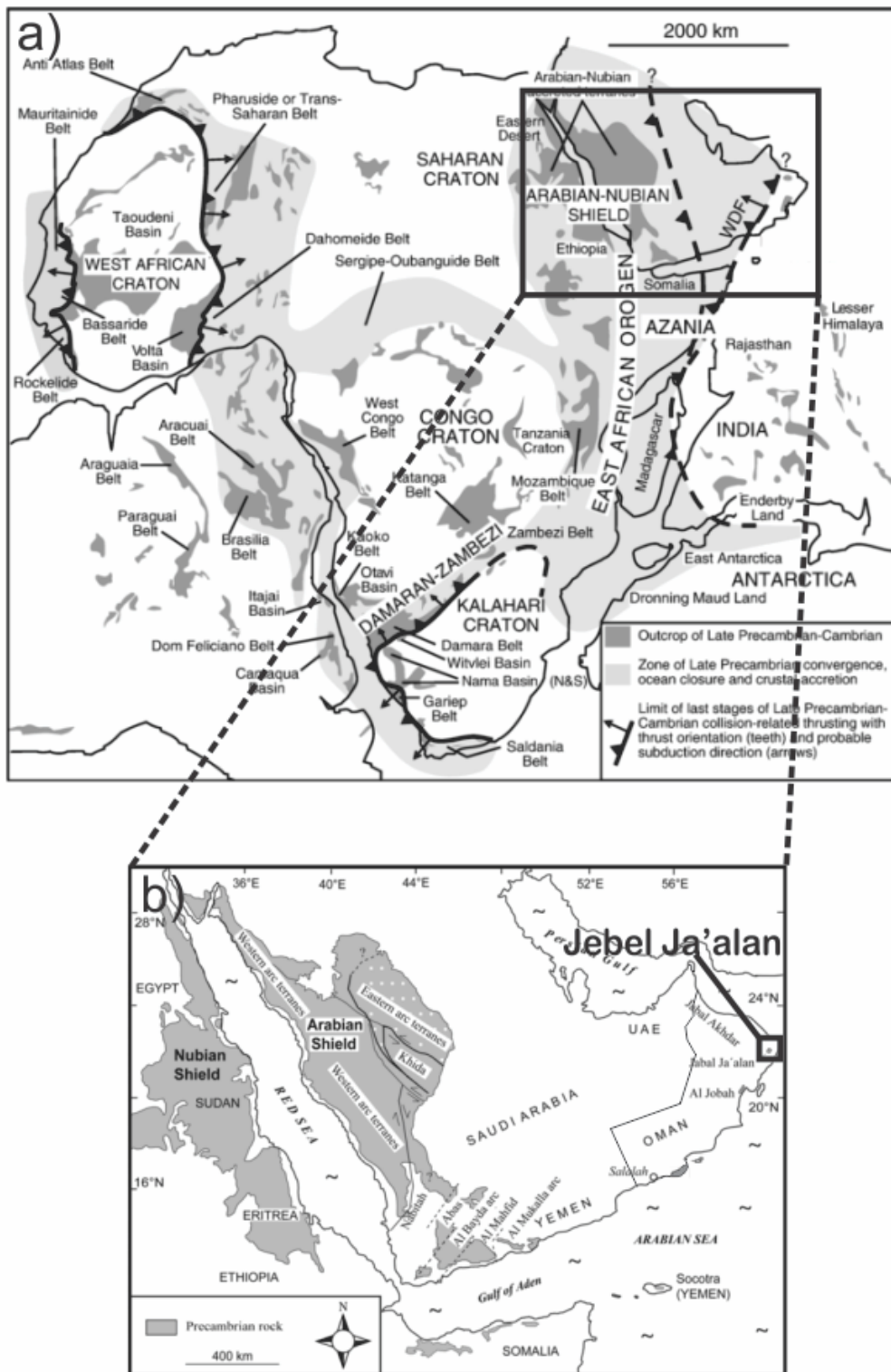
Figure 1: a) Reconstruction of Gondwana at 540 Ma (modified from Allen 2007) showing outcrops of Neoproterozoic rock and sutures and the main orogens and shields of Gondwana. b) A map of the Arabian Peninsula showing the location of the Arabian-Nubian Shield, Oman and the study area of this project (modified from Rantakokko et al. 2014).

GEOLOGICAL SETTING

Location

The study area (figure 2) of this project is located in Jebel Ja'alan, 50 km SSW of Sur, Sultanate of Oman (figure 1b). This area is partly made up of an inlier of basement rock surrounded by Cenozoic sediments. It makes up one of only a few occurrences of basement in Oman compared to the more well exposed basement of Saudi Arabia and Yemen to the west (Gass et al. 1990).

Rock Types

Jebel Ja'alan contains a large and diverse array of lithologies up to Neoproterozoic in age. The oldest rocks of the area, as interpreted by field relationships, are metasedimentary gneisses and schists seen predominantly on the northern side of the mountain with some smaller occurrences of metamorphosed granodiorite, granite, diorite and hornblendite (Gass et al. 1990). In the foothills on the southern side of the mountain, a large granite pluton was emplaced within the aforementioned metasediments. This intrusive body is cross-cut by several distinct dyke generations, most of which are doleritic but also some of intermediate chemistry. This particular project focuses on the suite of igneous rocks found in southern Jebel Ja'alan.

Age

The literature gives only one example of geochronologic data on the area: Gass et al. (1990) presented a Rb-Sr whole-rock isochron age from an igneous complex in Jebel Ja'alan of 850 ± 27 Ma, interpreted to be the age of crystallisation. In the same study, a mafic dyke of the area gave a K-Ar whole-rock age of 430 ± 20 Ma. From this small

suite of data it can be inferred that the large granite intrusion dominating the southern

area of Jebel Ja'alan was possibly emplaced during the Late Tonian to Early

Cryogenian, while one generation of the dyke swarm may have been emplaced during

the Silurian.
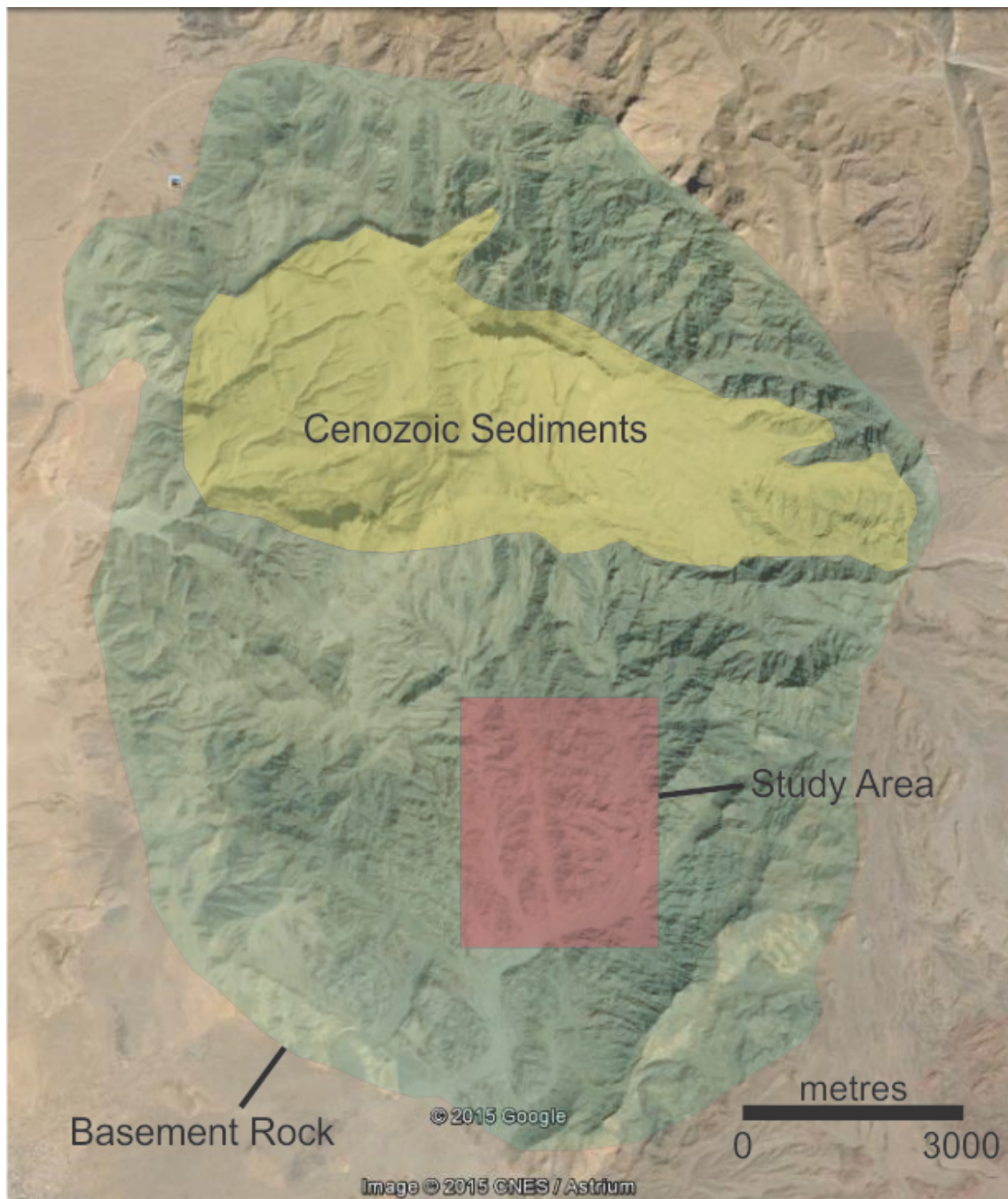
Figure 2: Image taken from Google Earth™ showing Jebel Ja'alan. The area of basement rock (green), the unconformable cenozoic sediments (yellow) at the summit of the mountain and the study area (red) are outlined.

History

Papers on other areas of exposed basement in Oman, namely the Mirbat region in the south, interpret the basement to have originated from a juvenile volcanic island-arc possibly occurring close to or at the margin of Neoproterozoic India (Rantakokko et al. 2014). Whether or not this island-arc is related to the amalgamated arc terranes of the Arabian-Nubian Shield cannot presently be confirmed because of the absence of basement rocks on the surface across a stretch of 800 km between the Mirbat region and the closest ANS outcrops (Rantakokko et al. 2014). The dyke swarms found on the southern foothills of Jebel Ja'alan are a common feature of the ANS (Worthing 2005, Ba-Bttat 1991). Worthing (2005) makes the point that the dyke swarms found in the Mirbat region were probably associated with a stage of extension following a collapse in the thickened lithosphere based on their sub-vertical angle and large thickness. Like the dyke swarm of Mirbat, the dykes of Ja'alan are NW-SE trending with a sub-vertical dip. The Sadh and Juffa Gneisses of Mirbat are calc-alkaline in nature and have similar U-Pb zircon ages to the Ja'alan Granite (Rantakokko et al. 2014, Gass et al. 1990). However, the Ja'alan Granite does not show metamorphic foliation and therefore must have been exhumed quickly after emplacement and post-dated the metamorphism of the gneisses and schists. The calc-alkaline suites associated with subduction in the western arc terranes of Saudi Arabia appear to be relatively coeval (~850 Ma, Robinson et al. 2014) with Mirbat (~835 Ma, Rantakokko et al. 2014) and Ja'alan (~850 Ma, Gass et al. 1990), indicating simultaneous arc magmatism across the Mozambique Ocean.

Following the island arc terranes of the Neoproterozoic, the next major geological event in Oman's history is the Huqf Supergroup deposited ca. 725 – 540 Ma. Its strata contain

glacial deposits and cap-carbonates overlain by siliciclastic and carbonate shelf

deposits, in turn overlain by evaporites, carbonates and organic-rich shales (Allen 2007,

Bowring et al. 2007, Leather et al. 2002, Allen et al. 2004, Allen et al. 2011). Such

deposits are indicative that late Neoproterozoic Oman was undergoing a period of basin

development following its initial accretion. Coeval magmatism across Oman at this time

may provide the evidence for the extension tectonics that facilitated the development of

the Huqf Basin (Rantakokko et al. 2014, Worthing 2005).

Much debate exists around the timing of Gondwana assembly, earlier papers

highlighting a more simplistic model of a fully amalgamated western Gondwana

colliding with a fully amalgamated eastern Gondwana, while other more recent papers

favour a longer lived, multi-stage assembly involving smaller terranes and continental

blocks (Meert 2003, Meert and Lieberman 2007, Meert and Van Der Voo 1997, Collins

and Pisarevsky 2005, Rogers et al. 1995). The ANS provides strong evidence for the

latter hypothesis because it is comprised of multiple sutured island-arc terranes, and by

extension, the Omani basement too, and therefore reflects multi-stage accretion. Meert

(2003) proposed that the eastern part of Gondwana amalgamated over an interval from

~750 Ma to ~530 Ma and therefore suggests that its assembly was concurrent with the

final assembly of Gondwana.

Constraining the age and setting of the Omani basement is important on a larger scale

for understanding the amalgamation of Gondwana. In turn, Gondwana is a very

important piece of Earth history as it marks the end of the severe glacial episodes of the

Neoproterozoic and ushers in the radiation of the Ediacaran and Cambrian fauna (Meert

and Lieberman 2007). It is easy to imagine a link between these significant events in evolution to the arrangements of the continents at the time (Bowring and Martin 1999). Meert and Lieberman (2007) postulate that the genesis of the East African, Brasiliano, Kuungan and Damaran orogenies changed ocean chemistry through erosion of mountain chains, creating a more nutrient-rich environment suitable for the development of fauna.

METHODS

Field work was undertaken in eastern Oman, in the foothills of Jebel Ja'alan. Field notes and diagrams were sketched to interpret the field relationships present. A geological map was also produced and 22 samples were collected for analysis in Adelaide.

Mineral separation and milling for geochemical and geochronological sampling was carried out in the Mawson Laboratories at the University of Adelaide. Rocks were cut into fist sized pieces using a diamond-coated rock-saw and then crushed to gravel using an iron jaw crusher. The granite samples were crushed in the disc mill and sieved using an auto-sieve for zircon separation. All samples were run through a tungsten carbide ringmill to produce a fine powder required for geochemical analysis. After crushing in the disc mill and sieving, the grains between 79 μm and 479 μm were separated by panning to remove the light weight minerals and run through a Frantz machine to remove the magnetic minerals. Methyl iodide was also used to further remove the minerals with a density less than 2.28 g/cm³. The remaining sample contained the zircons. Two of the granite samples yielded zircons, these were mounted and imaged using a Philips XL20 SEM with EDAX EDS and Gatan Cathodoluminescence (CL)

detector (Waite Campus, University of Adelaide). After imaging, the zircons were

analysed using New Wave 213 – 7500cx LA-ICP-MS at Adelaide Microscopy. The

zircons were further analysed to obtain Lu-Hf model ages using a LA-MC-ICP-MS at

CSIRO (Waite Campus).

All samples were geochemically analysed at CSIRO (Waite Campus) for major

elements using x-ray fluorescence (XRF), while trace element analysis was carried out

at Adelaide Microscopy using LA-ICP-MS. These analyses used XRF discs fused at

Mawson Laboratories.

Thermal Ionisation Mass Spectrometric analyses of Sm-Nd and Sr were carried out at

Mawson Laboratories on the two dolerite generations (JA15-14 and JA15-42), the

andesite (JA15-34), the hornblendite (JA15-25) and granite (JA15-18). The samples

were prepared from rock powders that were dissolved in acids and filtrated through

specialised columns to collect the Nd, Sm and Sr found within the rocks. Refer to

appendix A for a more detailed methodology.

OBSERVATIONS AND RESULTS

Field and Petrographic Observations

In the field, five main rock types were observed: granite, hornblendite, grey dolerite,

andesite and brown dolerite. Some of the field relationships are shown in figure 3.

JA'ALAN GRANITE

A pervasive granitic pluton that dominates the southern flank of Jebel Ja'alan, it is cross-cut by three obvious dyke generations (figure 3 and 4). There are occasional xenoliths of basement gneiss inside the granite. The primary minerals include quartz, plagioclase, K-feldspar, garnet ± muscovite and biotite. Most outcrops were leucocratic but there were occurrences of more pinkish granite too. A thin section of JA15-18 showed the minerals sphene, quartz, microcline, plagioclase, hornblende, zircon, chlorite replacing amphibole and notably very little mica, leading to the assumption that it is an I-type granite.

HORNBLENDITE

This was observed as a mafic intrusion within the granite forming 10 metre scale blobs, Gass et al. (1990) referred to it as hornblendite. Aerial photograph interpretation showed the hornblendite to be the dominant rock type in the south of figure 4. Minerals identified in the field were hornblende, plagioclase, quartz ± pyroxene. It was also observed to be covered with orange rust specks. No field relationship was able to be derived from the outcrops observed so it was impossible to comment on relative timing.

GREY DOLERITE

This was the first generation of dykes cross-cutting the granite pluton (figure 3a). It was sometimes observed to have a glomeroporphyritic texture of plagioclase phenocrysts. It was common to observe cracks in the dolerite to be filled with the granite. Many of the dykes showed magma mingling at their margins where an intermediate rock had crystallised between it and the granite. Compared to the later brown dolerite, the dykes

of this 1st generation had a shallower dip angle. Thin section observation showed it to have a plagioclase ± quartz and K-feldspar groundmass, hornblende, epidote and biotite.

ANDESITE

This is the 2nd dyke intrusion, showing evidence of cutting both the granite and the 1st dolerite. It was observed to be intermediate in mineralogy and colour and it was coarser grained than the dolerites. These dykes had a similar dip angle as the grey dolerite, suggesting that they are part of the same suite. Through thin section its mineralogy was deemed to be feldspar-rich, a crowded plagioclase-rich assemblage, hornblende replacing chlorite and sphene, magnetite and epidote as accessories. This led to the interpretation of the rock as an andesite.

BROWN DOLERITE

A dolerite that weathers to a brown colour but it is a dark grey when fresh. These dykes tended to be very steep angle, possibly suggesting emplacement during a phase of extension. They were also, on average, much thicker than the other dykes, reaching 15 m width. This made them easily recognisable in aerial photographs, where some were seen to be in excess of 1 km long (figure 4). Through thin section, JA15-42 was interpreted to be an anorogenic, alkaline dolerite containing sanidine and possibly nephylene. Due to their difference in dip angle, size and mineralogy, this generation is interpreted to be a different suite to the 1st dolerite and the andesite.
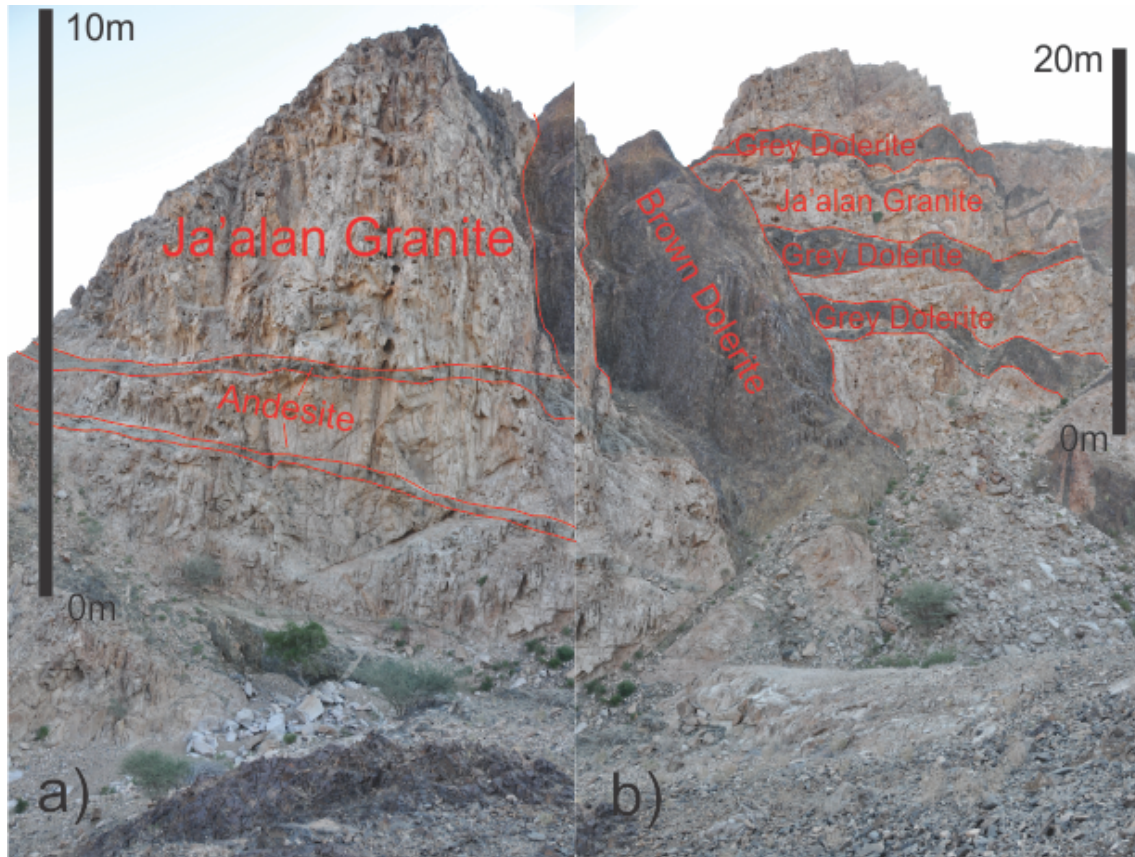
Figure 3: Field photos showing the cross-cutting relationships of each intrusion. UTM: Zone 40Q 0744600, 2450370. a) Shows the relationship between the Ja'alan Granite, andesite and brown dolerite. b) Shows the relationship between the Ja'alan Granite, grey dolerite and brown dolerite.
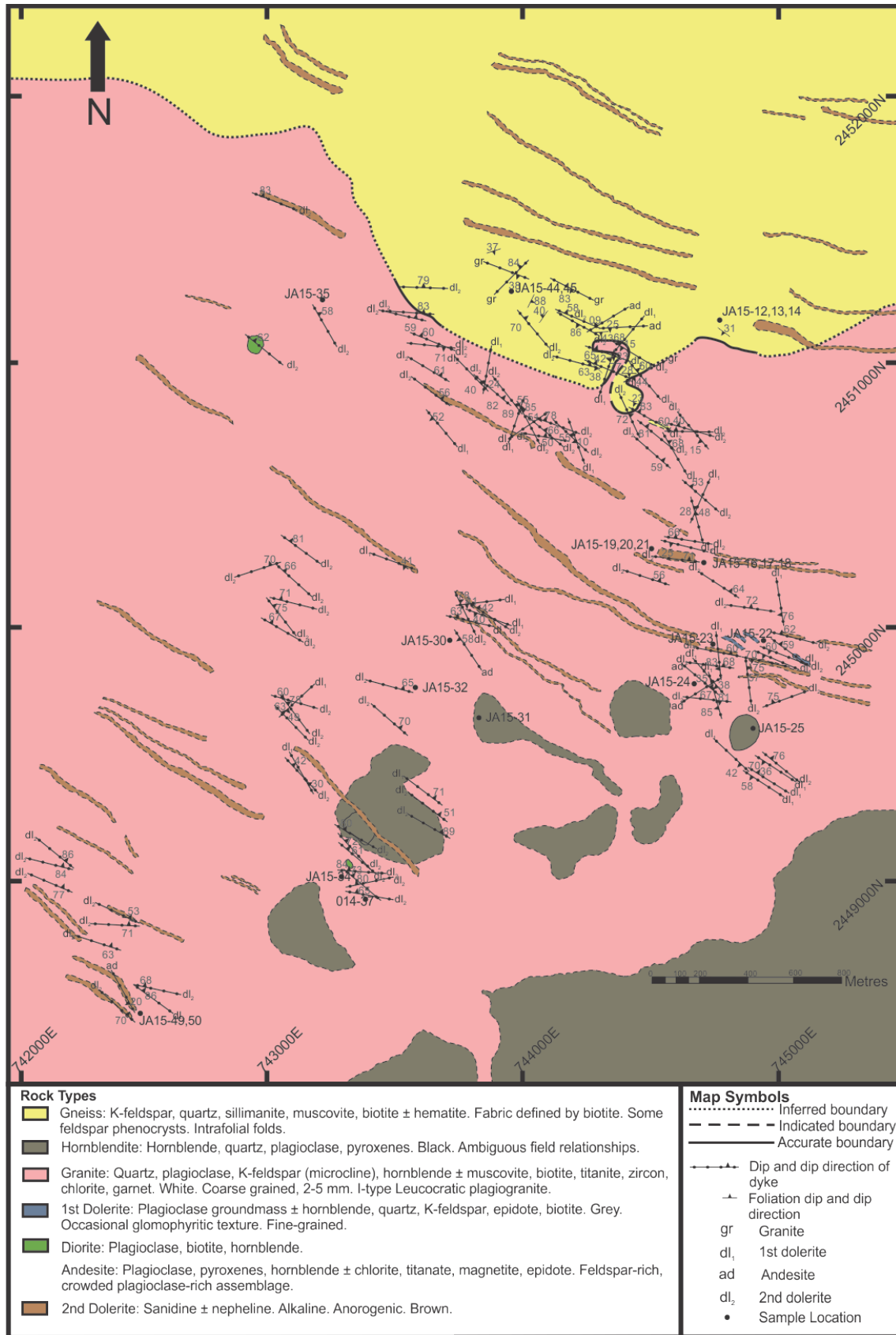
Figure 4: Geological map of field area located in the southern foothills of Jebel Ja'alan. The dominant lithology in pink represents the granite batholith, bounded in the south-east by the

hornblendite and in the north by the gneiss. The brown streaks represent 2nd generation dolerite drawn on from interpretation of Google Earth™ images.

U-Pb Geochronology

Samples JA15-33 (figures 5, 6 and 7) and O14-37 (figure 8, 9 and 10) were the only granite samples to yield zircons. They were both taken from the Ja'alan Granite Batholith. Most grains in both samples showed oscillatory zoning, indicating formation in a magma chamber (figures 7 and 10) (Corfu et al. 2003). Most analyses were targeted at the rims. Forty-four spots on 44 zircons were shot from O14-37. Of these, five were >90% concordant, so analyses with >75% concordance were also plotted (figure 5). The five grains selected gave a mean ^{206}Pb/^{238}U age of 843 ± 20 Ma with 95% confidence and a mean square weighted deviation (MSWD) of 2.0 (figure 6). Forty-two spots on 41 zircons were shot for JA15-33. Nine of the analyses were >90% concordant. These spots gave a weighted average ^{206}Pb/^{238}U age of 835 ± 35 Ma with 95% confidence and a MSWD of 14. Because the MSWD was high, the outer lying data were removed to leave five ages, giving an average of 837 ± 36 Ma with 95% confidence and a MSWD of 5. 9 (figure 9). High ^{204}Pb counts were recorded, which is interpreted to account for much of the discordance in the data.
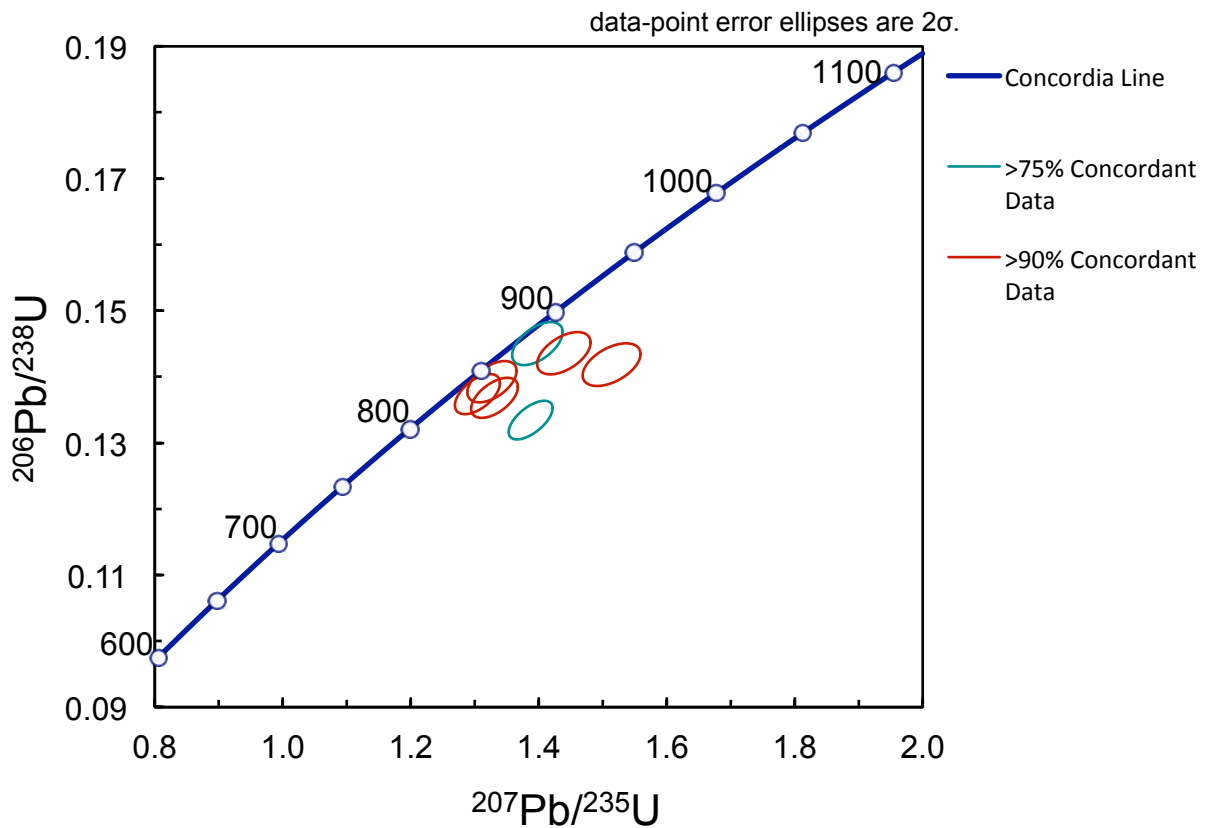
Figure 5: U-Pb concordia graph for sample O14-37 of the Ja'alan Granite showing the most concordant ages from the data. The data point error ellipses are to 2σ.
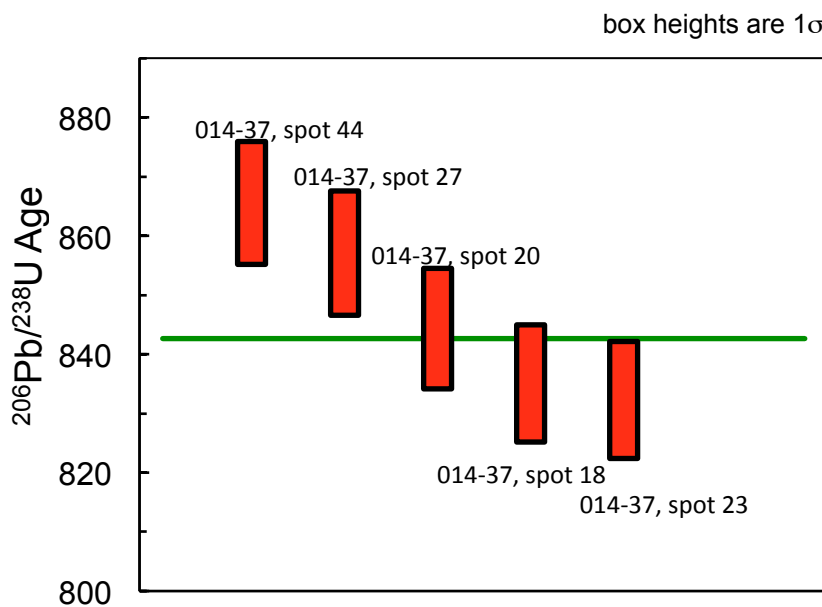
Figure 6: A weighted average plot illustrating the average $^{206}Pb/^{238}U$ age for O14-37 according to the five most concordant data spots. The heights of the box plots are to 1σ. The average $^{206}Pb/^{238}U$ age is 843 ± 20 Ma.
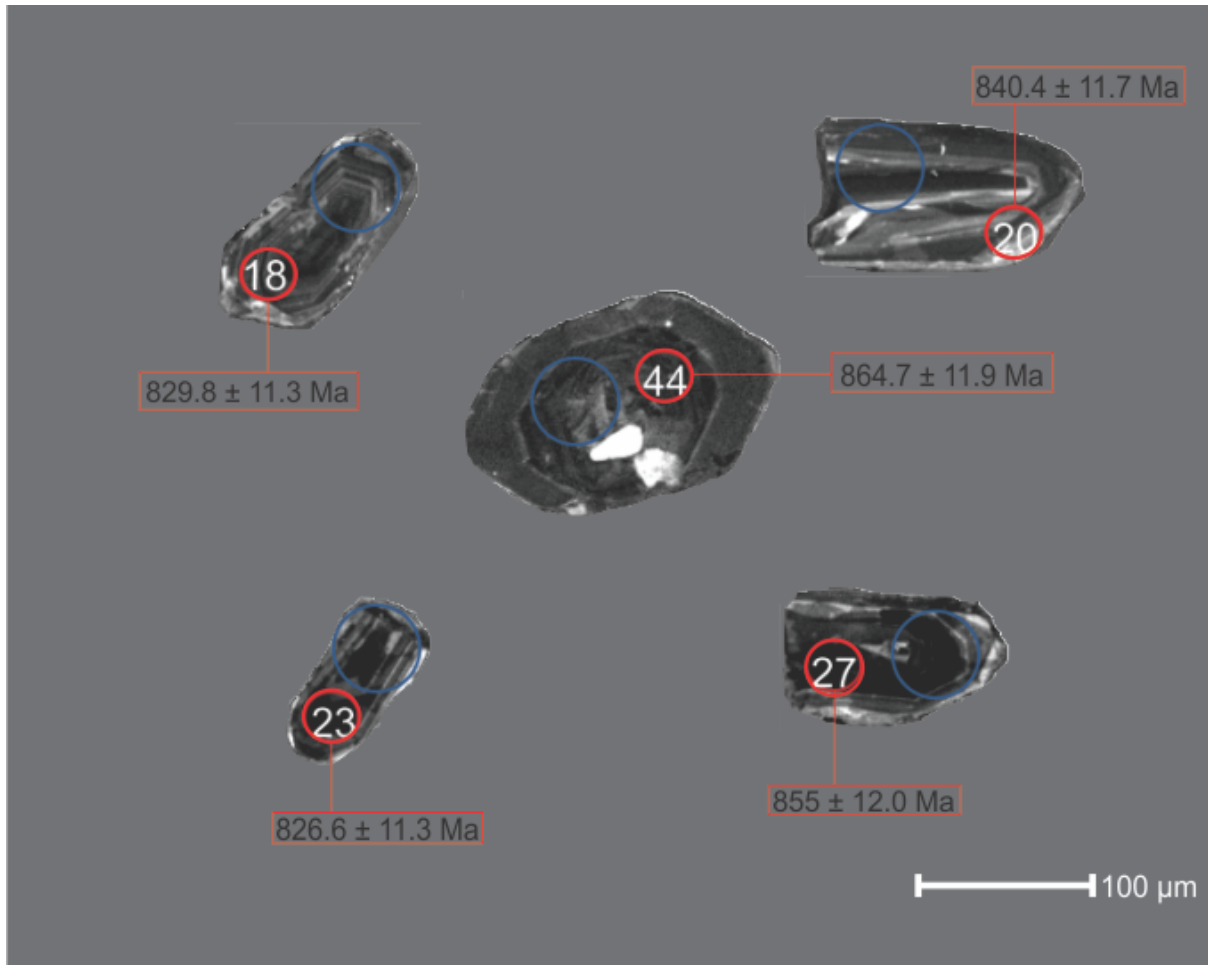
Figure 7: CL images of zircons from O14-37. Red circles represent U-Pb LA-ICP-MS spot locations. Blue circles represent Lu-Hf MC-LA-ICP-MS spot locations. Zircons show oscillatory zoning symptomatic of formation within a magma chamber. Dark zones in grains suggest higher uranium concentrations.
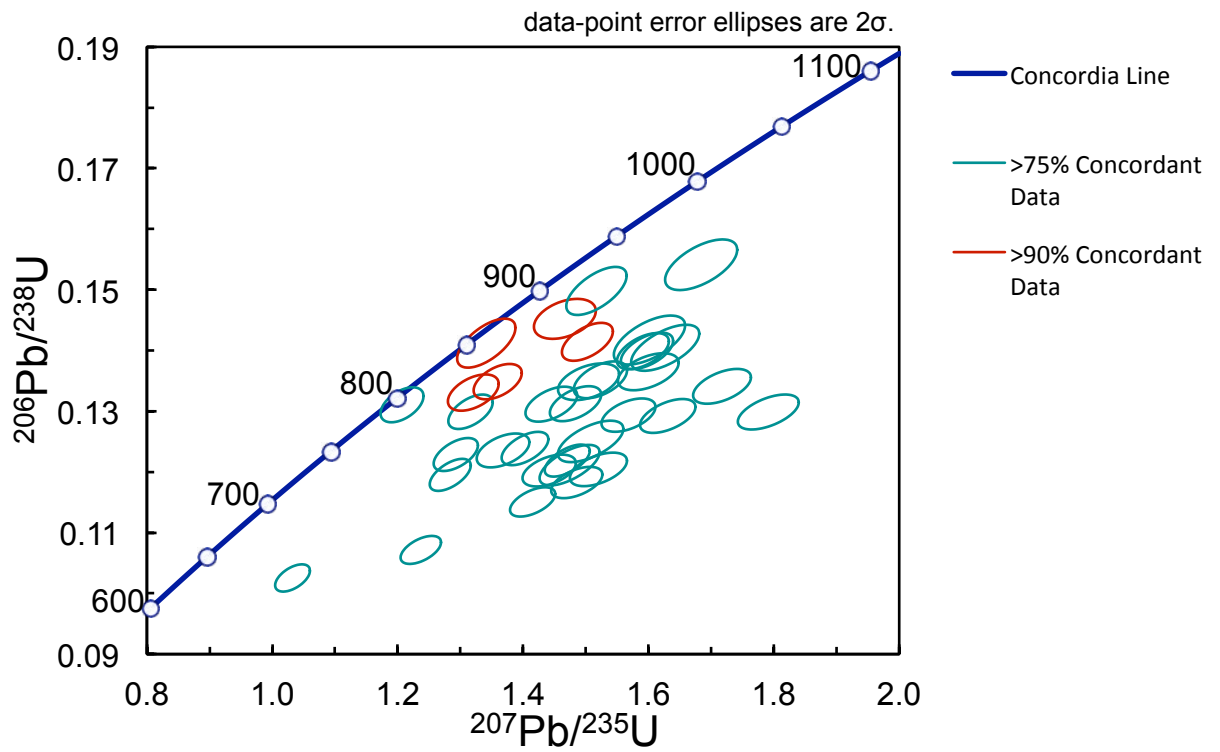
Figure 8: U-Pb concordia graph for sample JA15-33 of the Ja'alan Granite showing the most concordant ages from the data. The data point error ellipses are to 2σ.
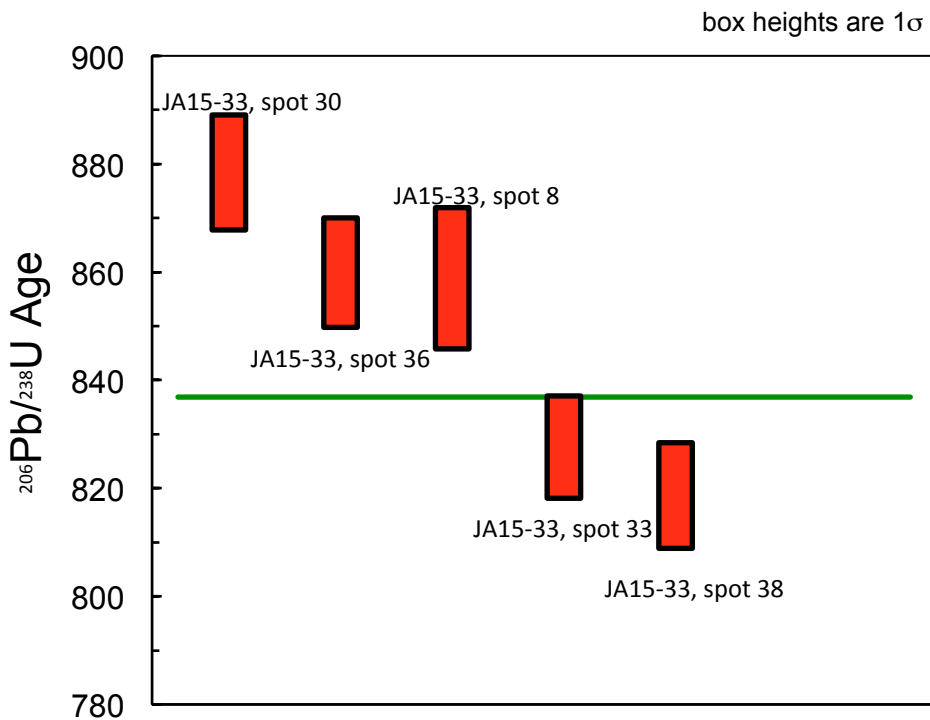
Figure 9: A weighted average plot illustrating the average ^{206}Pb/^{238}U age for JA15-33 according to the five most concordant data spots. The heights of the box plots are to 1σ. The average ^{206}Pb/^{238}U age is 837 ± 36 Ma.
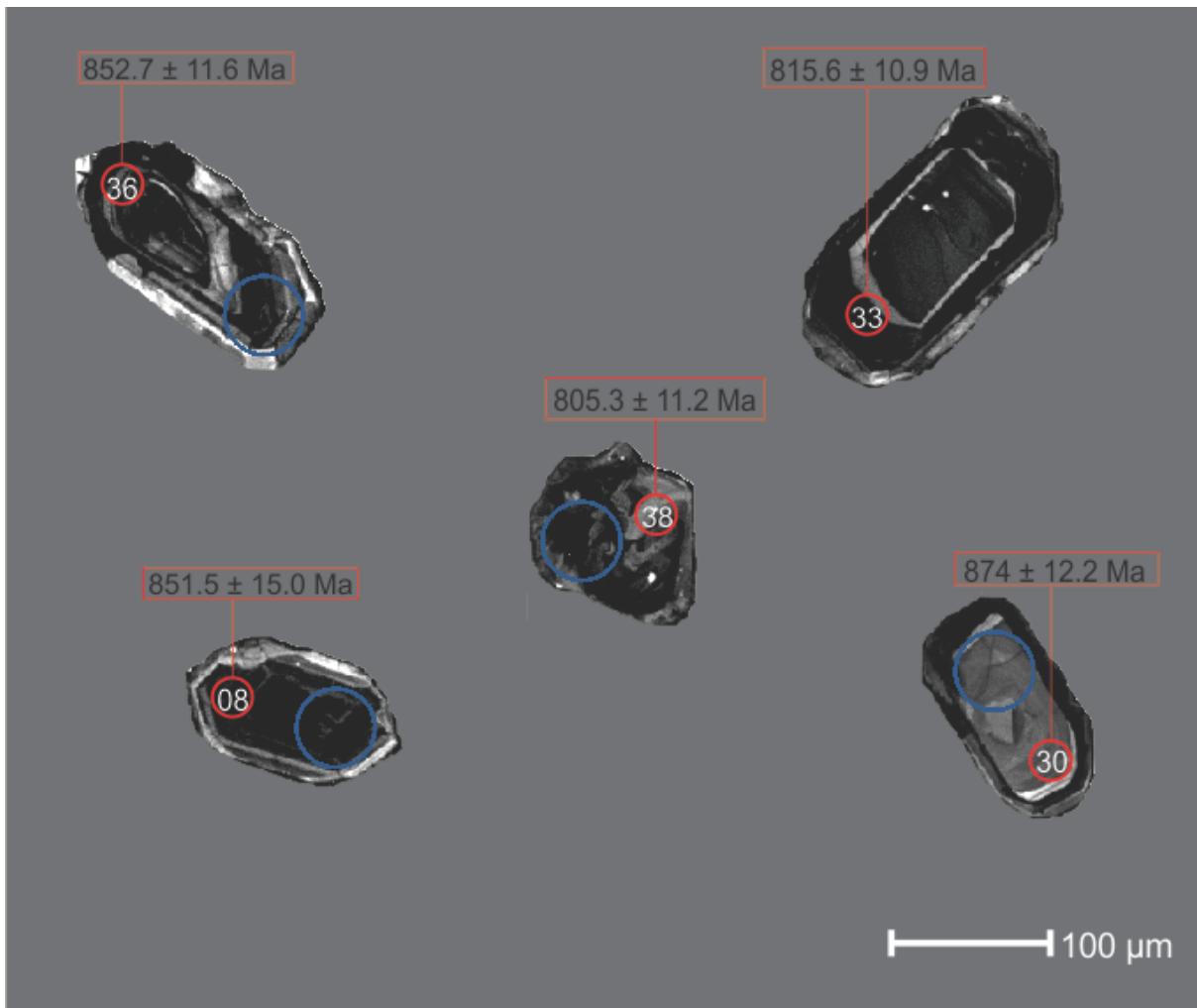
Figure 10: CL images of zircons from JA15-33. Red circles represent U-Pb LA-ICP-MS spot locations. Blue circles represent Lu-Hf MC-LA-ICP-MS spot locations. Zircons show oscillatory zoning symptomatic of formation within a magma chamber. Dark zones in grains suggest higher uranium concentrations.

Zircon Lu-Hf Geochronology

The Lu-Hf method is very useful in the study of the origin of igneous rocks. ^{176}Lu decays by β-emission to the stable isotope ^{176}Hf. Because Lu is a compatible element to the solid mantle and Hf is incompatible, igneous rocks are relatively concentrated in Hf and depleted in Lu compared to the depleted mantle. Using this knowledge, ^{176}Lu/^{176}Hf ratios allow for accurate dates for when the rock-forming melt left the mantle. The

highest concentrations of hafnium occur in zirconium minerals, e.g. zircon (Faure and

Mensing 2005). Because of zircon's resistance to weathering, it provides a virtually

unaltered record of hafnium evolution in the rock. Eight zircons from sample O14-37

(Ja'alan Granite) were analysed based on their concordance from U-Pb analyses. Six of

the eight spots returned positive εHf values ranging between +4.55 and +9.92. The two

other zircons provided counts that were too high to provide accurate data. Because the

values lie between the depleted mantle evolution line (DM) and the chondritic uniform

reservoir (CHUR) it can be suggested that O14-37 originated from a juvenile source

(figure 11). Eleven zircons from JA15-33 were analysed based on the most concordant

analyses from the U-Pb analyses. All analyses returned positive εHf values ranging

between +2.30 and +10.17 (table 1), therefore the samples were enriched in ^{176}Hf

compared to CHUR (Faure and Mensing 2005). Like O14-37, all the εHf values lie

between the DM and CHUR and can be interpreted to be juvenile (figure 11).

Table 1: A table of zircon Lu-Hf results shown with each zircon's respective ^{206}Pb/^{238}U age.

Sample	U/Pb AGE	εHf	1s	T(DM)	T(DM) (Ga)	Hf Chur (t) (Crustal)	Hf DM (t)
O1437-07	873	8.832311	1.791521	1.067652	1.179890243	0.282233466	0.28262
O1437-18	830	4.552549	3.741535	1.215282	1.413564979	0.282260842	0.28265
O1437-20	840	9.915661	0.817399	0.990979	1.085878875	0.282254478	0.28264
O1437-23	827	7.043952	2.021053	1.099418	1.255563784	0.282262752	0.28265
O1437-27	855	8.928956	2.250686	1.053434	1.159614581	0.282244928	0.28263
O1437-44	865	5.336131	0.729704	1.192593	1.392090231	0.282238561	0.28262
JA1533-04	900	6.751777	0.669707	1.167074	1.331242171	0.282216264	0.28260
JA1533-07	835	5.771298	1.365062	1.150988	1.341405966	0.28225766	0.28264
JA1533-08	851	2.299765	1.906975	1.312499	1.570254239	0.282247475	0.28263
JA1533-19	787	5.581971	1.078304	1.116233	1.315607836	0.282288197	0.28268
JA1533-21	835	5.515733	0.845042	1.162179	1.357366283	0.28225766	0.28264
JA1533-24	794	7.21626	2.410219	1.06875	1.218820259	0.282283746	0.28267
JA1533-30	874	10.17285	1.197695	1.012208	1.096678267	0.282232829	0.28261
JA1533-31	835	8.505385	2.659206	1.056516	1.17036092	0.28225766	0.28264
JA1533-36	853	5.732376	1.187737	1.176753	1.357955028	0.282246202	0.28263
JA1533-37	835	4.583765	1.533764	1.200173	1.415528615	0.28225766	0.28264
JA1533-38	805	3.446748	1.202722	1.214273	1.463000121	0.282276749	0.28267
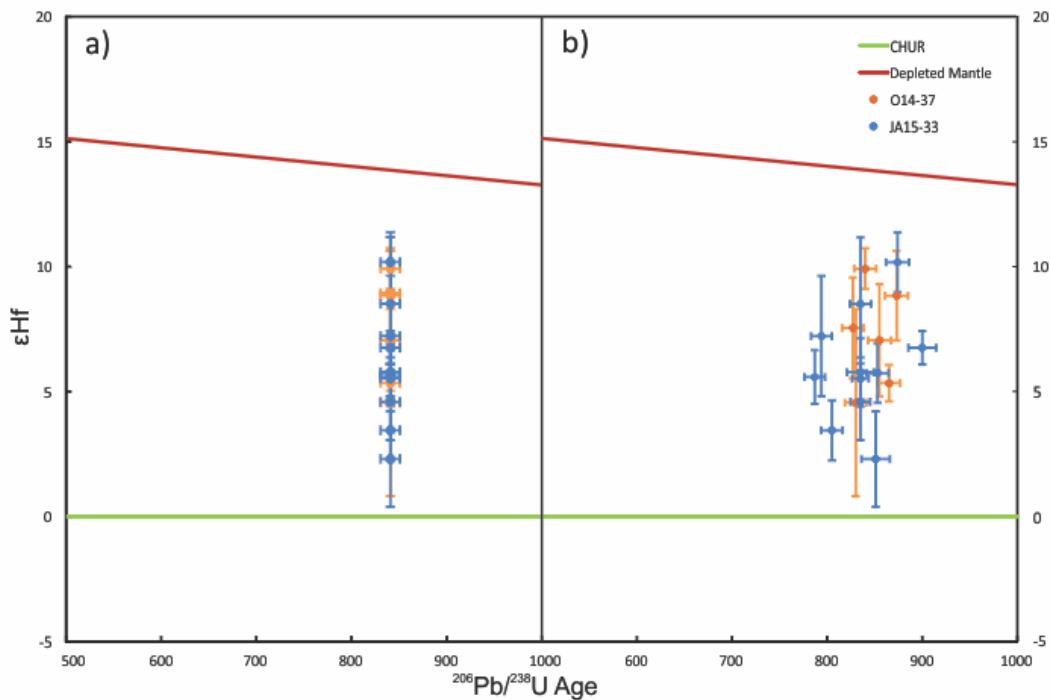
Figure 11: εHf versus ²⁰⁶Pb/²³⁸U age plot. The green line along the x-axis represents the chondritic uniform reservoir. The red line represents the depleted mantle. The orange population is zircon laser spots from sample O14-37. The blue population is zircon laser spots from sample JA15-33. a) Shows the data points plotted at an arbitrary 840 Ma age to represent the interpreted age of Ja'alan Granite crystallisation. b) Shows the data plotted according to their respective zircon ²⁰⁶Pb/²³⁸U ages.

Sm-Nd Radiogenic Isotopes

The Sm-Nd system is highly applicable to old rocks because unlike Rb, Sr, Th, U and

Pb, Sm and Nd are highly immobile and can therefore be used to see through the

younger events that may have affected the chemistry of other systems (Rollinson 1993).

Five samples were selected, each representing the five dominant rock types of southern

Jebel Ja'alan, for Sm-Nd isotope analysis. All five samples gave positive εNd values

between +0.56 and +6.78 (table 2) and plotted between the depleted mantle line and the

CHUR line indicating a juvenile nature (figure 12). The isotopic evolution of JA15-18

(granite) is plotted on figure 12, showing the depleted mantle model age as 1291 Ma

and the εNd (t=0) as -8.23. Comparing this to the U-Pb age 843 ± 20 Ma of JA15-33,

the relative proximity of these ages is further evidence of a relatively juvenile origin of the intrusive rocks. The DM model ages of the other rocks are all Mesoproterozoic age and older than the granite model age despite field relationships showing that they were emplaced after the granite. Most notably, the latest intrusion (JA15-42) has the oldest model age (1663 Ma).

Table 2: A table of results for Sm-Nd analysis of unknowns and standards. The U-Pb age of the granite has been used for all samples as a maximum age of crystallisation.

Sample	(STD) BCR-2	(STD) G-2	JA15-14	JA15-18	JA15-25	JA15-34	JA15-42
Input age of rock T (Ma)	**840**	**840**	**840**	**840**	**840**	**840**	**840**
Unmixed 143/144Nd	.512628	.512217	.512965	.512216	.512629	.512615	.512375
Nd ugg^{-1}	28.8	52.3	11.5	23.7	27.2	37.6	58.8
Sm ugg^{-1}	6.8	7.9	3.7	4.1	7.3	9.5	14.0
147Sm/144Nd	.1423	.0916	.1930	.1044	.1616	.1523	.1436
εNd (T=0)	-.19	-8.21	6.39	-8.23	-.17	-.44	-5.14
143Nd/144Nd (T)	.511844	.511713	.511902	.511639	.511739	.511776	.511584
εNd (T)	5.65	3.09	6.78	1.72	3.59	4.32	.56
TDM (Ma)	1102	1156	1310	1291	1499	1309	1663
TCHUR (Ma)	28	611	-14720	698	39	79	758
DM at age of rock (T)	.511968	.511968	.511968	.511964	.511968	.511968	.511968
CHUR at age of rock (T)	.511555	.511555	.511555	.511551	.511555	.511555	.511555
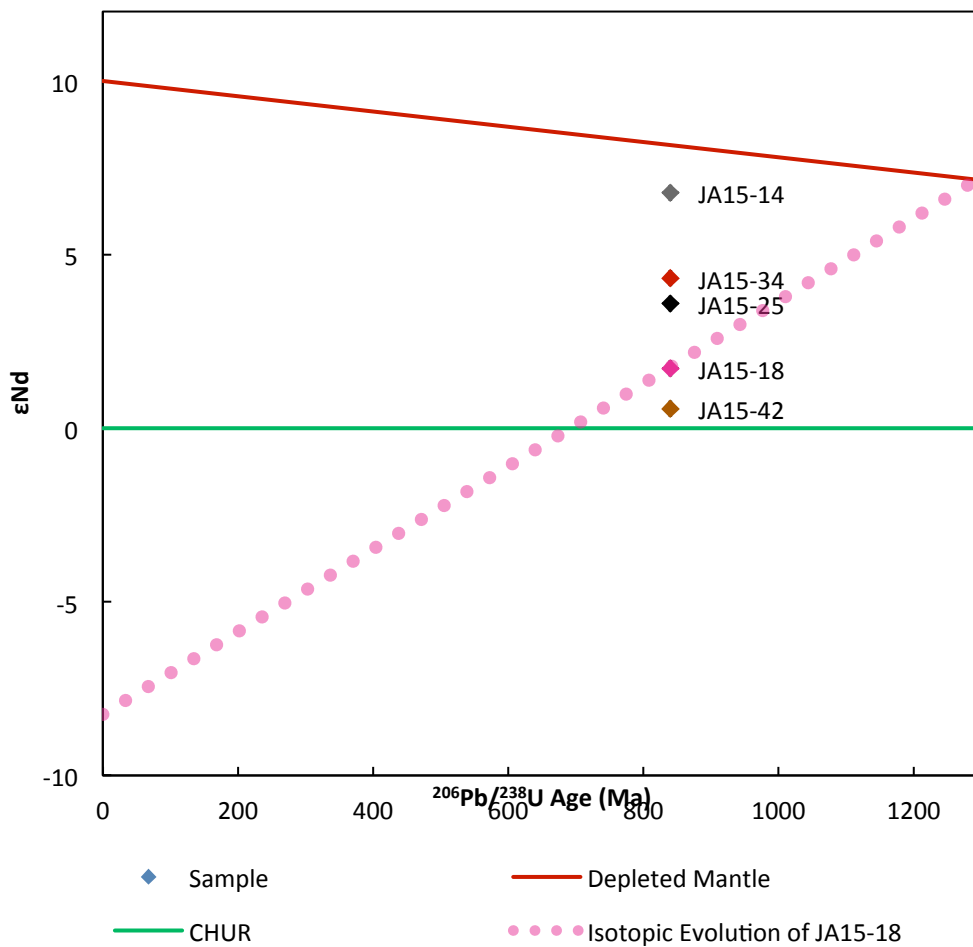
Figure 12: εNd versus time plot showing samples JA15-14 (grey dolerite), JA15-18 (Ja'alan Granite), JA15-25 (hornblendite), JA15-34 (andesite), JA15-42 (brown dolerite). The red line represents the evolution of the depleted mantle. The green line represents CHUR. The isotopic evolution of JA15-18 (Ja'alan Granite) has been plotted in pink where the DM model age = 1291 Ma and εNd (t=0) = -8.23.

Major Element Geochemistry

Major element geochemistry is used widely in igneous petrology to classify rocks, especially with the advent of XRF analysis, major geochemical analyses can produce large volumes of data (Rollinson 1993). XRF analysis was undertaken on fused discs made at Mawson Laboratories for each sample collected in the field. The suites that were observed in Jebel Ja'alan were all interpreted to be plutonic, therefore a TAS plot

for plutonic rocks (Middlemost 1994) and a plutonic chemical variation diagram (De la Roche et al. 1980) have been used to classify the collected samples.

The three granite samples (O14-37, O14-35 and JA15-33) plotted on the far right of the TAS diagram (figure 13). O14-37 sits in the middle of the granite field, while O14-35 and JA15-33 lie within the quartz monzonite field. This fits well with field interpretations as these samples contain the most SiO_2 and are therefore the most felsic. The andesite dyke samples JA15-24 and 46 plot closely in the top of the granodiorite field, while JA15-34 contains 12-15% less SiO_2 than the other two and lies disparate in the monzodiorite field. For the brown dolerite samples, JA15-21 lies in the monzonite field but is separated from the other brown dolerites by at least 7% SiO_2. JA15-49 plots within the gabbroic diorite field, while samples JA15-13 and JA15-42 straddle the boundary between alkalic gabbro and gabbro. Samples JA15-17 and JA15-20 of the grey dolerite dyke swarm sit in the monzodiorite field, while JA15-14 and JA15-50 straddle the alkalic gabbro and gabbro fields like the brown dolerite phase. The granodiorite dyke sample JA15-12 plots on the TAS plot in the monzogabbro field, suggesting poor identification in the field. The two samples of the hornblendite plot in the alkali gabbro and gabbro fields.

Figure 14 is also a rock classification diagram. This classification is based off of cations, rather than weight % oxide data and is suggested by some to better represent cation distribution through a rock sample. In this case, figure 13 and 14 agree for most samples.
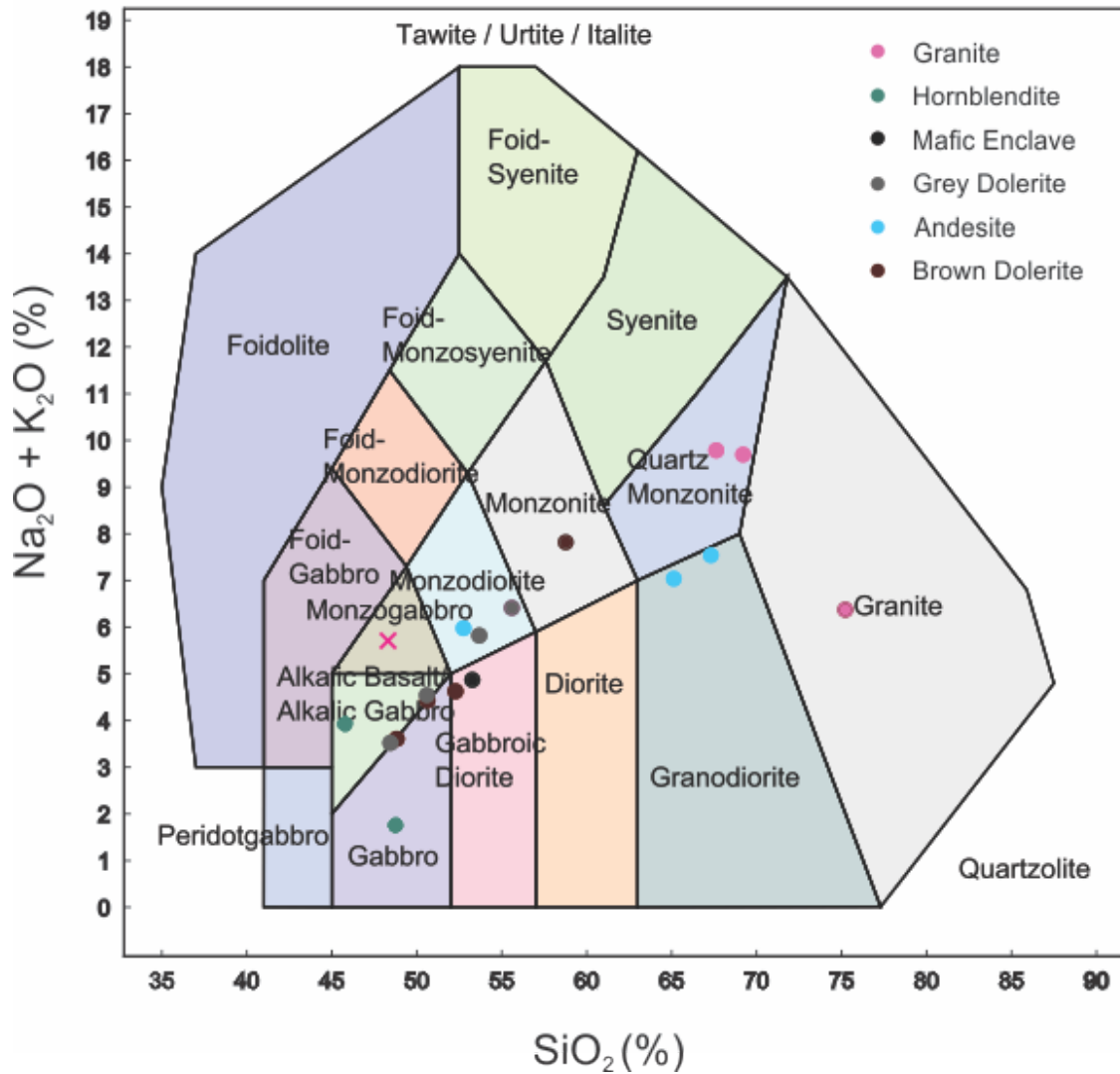
Figure 13: TAS plot for plutonic rocks (Middlemost 1994). Concentrations are based off X-ray fluorescence data. Granodiorite is plotted as a cross rather than a circle because, according to this plot, it has been misclassified.
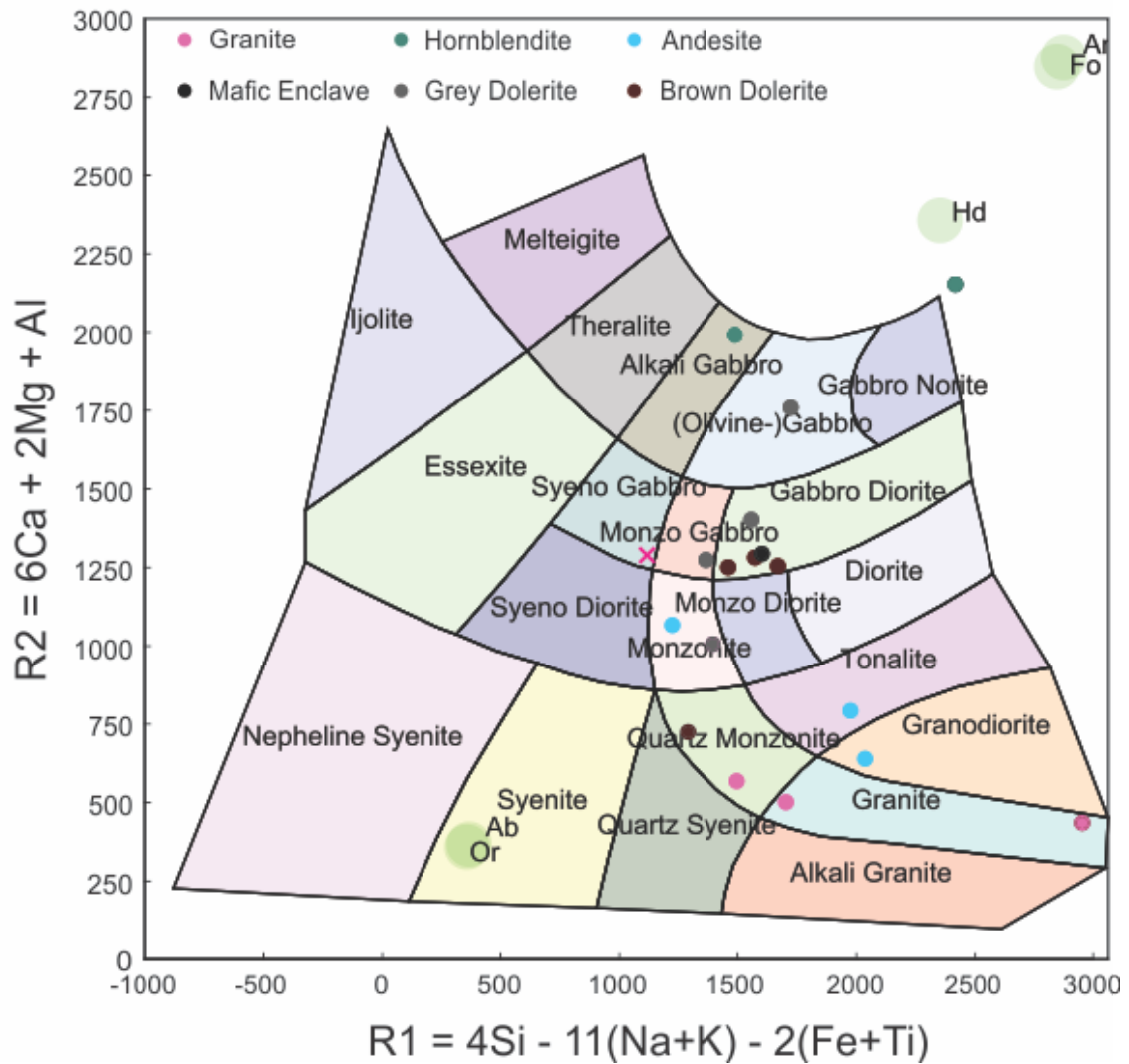
Figure 14: R1-R2 plutonic chemical variation diagram (De la Roche et al. 1980). Here, rock compositions are recalculated as cations. The weight percentage of the oxide is divided by the equivalent weight of the oxide set to one cation (Rollinson 1993). For example, the weight percentage of SiO_2 is divided by 60.09. The granodiorite sample has been plotted as a cross because it would appear not to be a granodiorite by this classification.

4.6 Trace Element Geochemistry

Trace elements are those elements that are present in a rock in concentrations of less

than 1000 ppm. These are vital in petrologic studies and are much better at

discrimination than major elements. In this study the trace elements were analysed on a

LA-ICP-MS using the left over discs from XRF analysis of major elements.

Figure 15 is a rare earth element (REE) spider plot that shows how enriched or depleted

in the REEs each sample is, compared to the values of the average chondrite according

to Boynton (1984). The y-axis is in logarithmic scale with the average chondrite line

intercepting the y axis at 1. Along the x-axis are the REEs - excluding Pm – in order of

atomic number.

Of the exposed complex, the andesite dykes are the most highly enriched in the lightest

REEs from La to Pr but for the rest of the elements values are relatively close to the

chondritic normal. The granites are also quite highly enriched in the light REEs but are

either depleted or close to average chondrite abundance for the rest of the element suite.

JA15-33 is rather anomalously depleted in the heavy REEs when compared to the other

two samples and it is in fact the most depleted sample in the entire suite. The grey

dolerites are mostly enriched in the light REEs but are close to the chondritic normal for

Gd to Lu. The brown dolerites are 5 to 10 times more abundant in La than the average

chondrite. With increasing atomic number, abundances steadily decrease - apart from a

spike in Eu for one sample – to the point where the heavy REEs are only 1 to 4 times

more abundant in the brown dolerite samples. The hornblendites are negligibly enriched

in some of the light REEs but, most noticeably, are the most depleted in the heavy REEs

apart from JA15-33 of the granites. Some of the granites, dolerites and the mafic

enclave show a negative Eu anomaly which is indicative of intracrustal melting, leaving

Eu in a plagioclase phase and depleting the melt.

All the samples have an overall inverse correlation between atomic number and enrichment of REEs. Enrichment and depletion is controlled by the minerals crystallising from the parent melt. In this case, where the heavy REEs are depleted in comparison to the lights, garnets in mafic and felsic liquids and hornblendes in felsic liquids may be responsible. For example, garnet in a basaltic liquid has a partition coefficient 1000 times greater for Lu than that for La (Rollinson 1993).

Some elements can be used to discriminate between different tectonic environments. The best elements for these analyses are the high field strength elements (HFSE), especially Ti, Zr, Y, Nb and P because of their insensitivity to secondary processes like hydrothermal, sea-floor weathering and medium grade metamorphism (Rollinson 1993). Figures 16 to 18 are basalt discrmination diagrams that are most helpful in discrimination when analysing mafic rocks. Hence the granites and the intermediate samples are not represented on these figures. However figure 17 does show the intermediates and felsics, because Th, Hf and Ta are also used for tectonic discrimination in granites.

Figure 16 does not give a clear discrimination for the Jebel Ja'alan samples. Three samples plot outside the tectonic fields, while the rest straddle the boundaries of within-plate basalt (WPB), calc-alkaline basalt (CAB) and mid-ocean ridge basalt (MORB) etc. Figure 17 illustrates that the samples have a strong affinity for the volcanic arc basalt (VAB) fields and, in particular, the CAB division. The Cabanis and Lecolle (1989) diagrams (figure 18) plots the samples in a similar way to the Wood (1980) diagram,

where all the samples are within the "arc" section. Seven of the eleven points plot in the

calc-alkaline section. This shows strong agreement between figure 17 and 18.

Figure 19 and figure 20 are both tectonic discrimination diagrams for granitic rocks by

Pearce et al. (1984). Figure 19 plots Y+Nb against Rb. Care must be taken when

reading plots containing Rb, as it is quite a mobile element and current concentrations

may not reflect concentrations at the time of crystallisation. O14-35 and O14-37 both

plot in the bottom left of the volcanic arc granite field due to low concentrations in all

three elements. The other granite sample, JA15-33, does not plot on the diagram at all

due to even lower levels in Y, Nb and Rb. The Ta vs Yb plot (figure 20) shows the same

results as figure 19. O14-35 and 37 plot in the VAG field, while JA15-33 plots outside

the diagram due to very low concentrations of Yb and Ta.
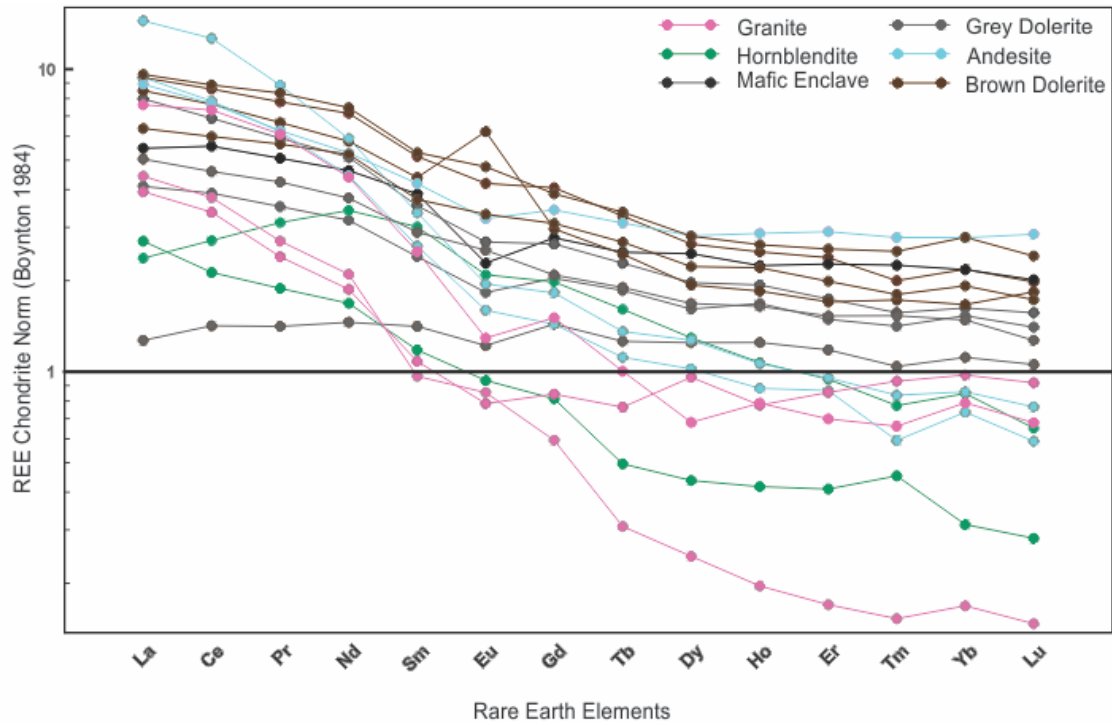
Figure 16: Rare earth element (REE) spider plot normalised to the average chondrite meteorite (Boynton 1984). Plotted above are all the samples analysed for trace elements including: 3 granites, 4 grey dolerites, 4 brown dolerites, 2 hornblendites, 2 andesites and 1 mafic enclave from within the granite pluton.
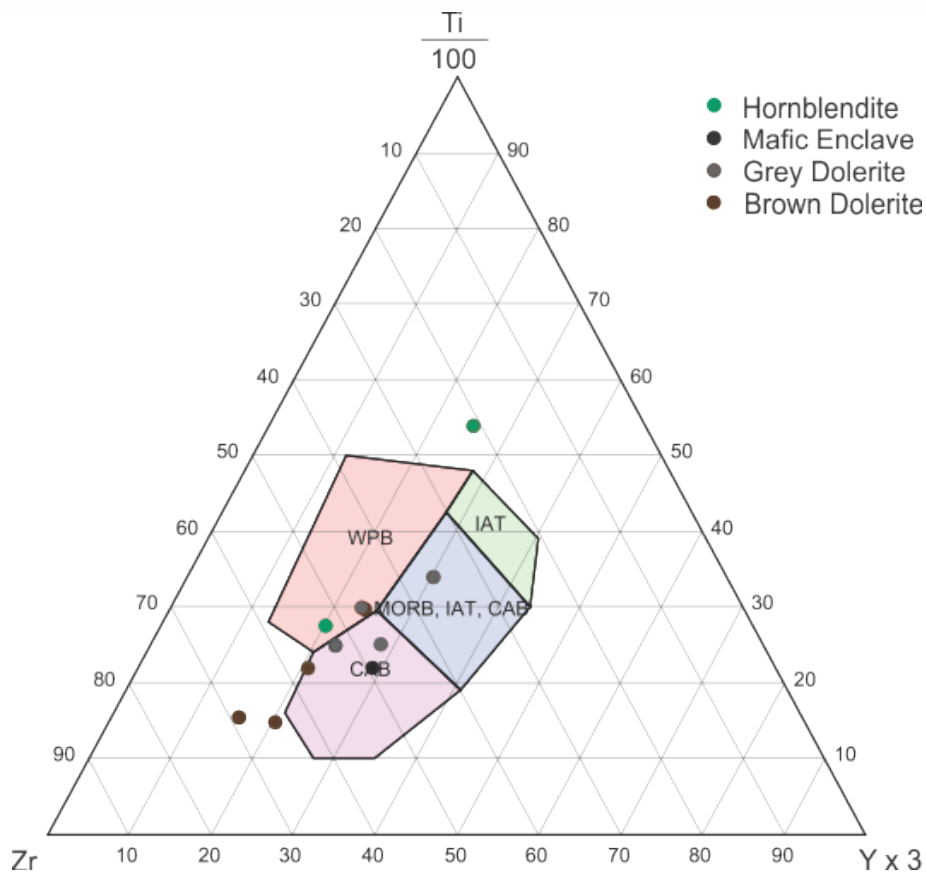
Figure 15: A ternary plot for tectonic classification of basalts measuring Ti/100, Zr, and Yx3 (Pearce and Cann 1973). There are four tectonic classifications shown on the diagram: "calc-alkaline basalt (CAB)", "within-plate basalt (WPB)", "mid-ocean ridge basalt (MORB), island-arc tholeiite (IAT), CAB" and "IAT". Only the mafic rocks of the suite have been plotted because of the specificity of the diagram.

35
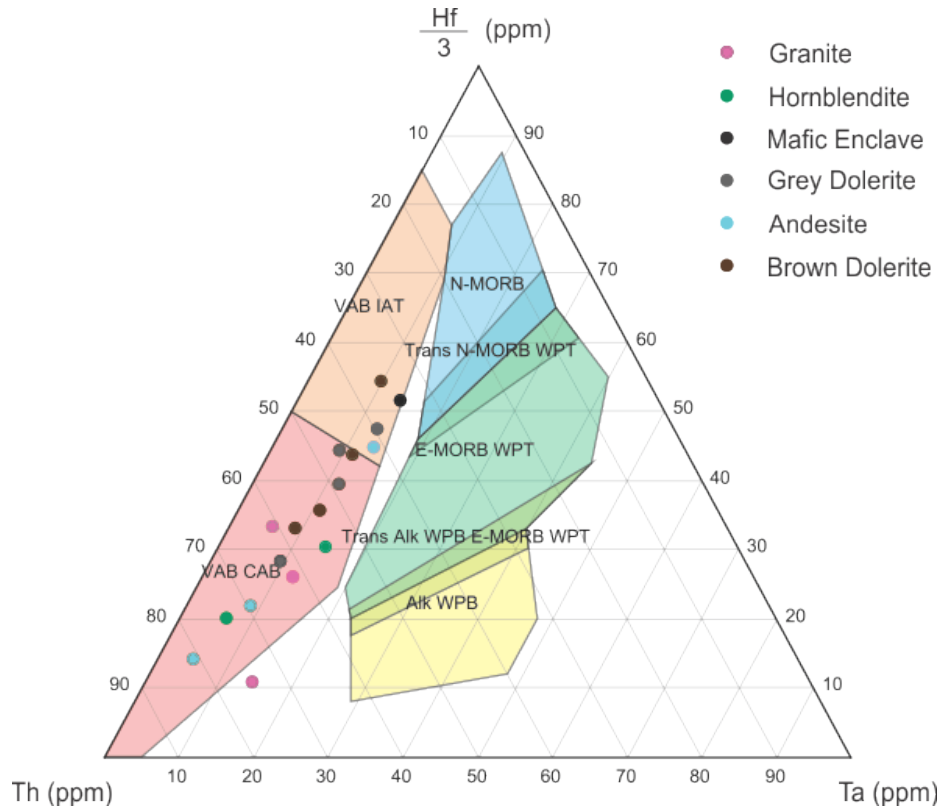
Figure 17: A basalt tectonic discrimination plot that uses the HFS elements Th, Hf and Ta (Wood 1980). The fields where the majority of the samples plot are volcanic arc basalt fields (VAB), which are separated into calc-alkaline basalt (CAB) and island arc tholeiite (IAT). It was decided to add the granite and andesite samples to this plot because the Wood (1980) discrimination diagram can be applied to intermediate and siliceous liquids too (Rollinson 1993).
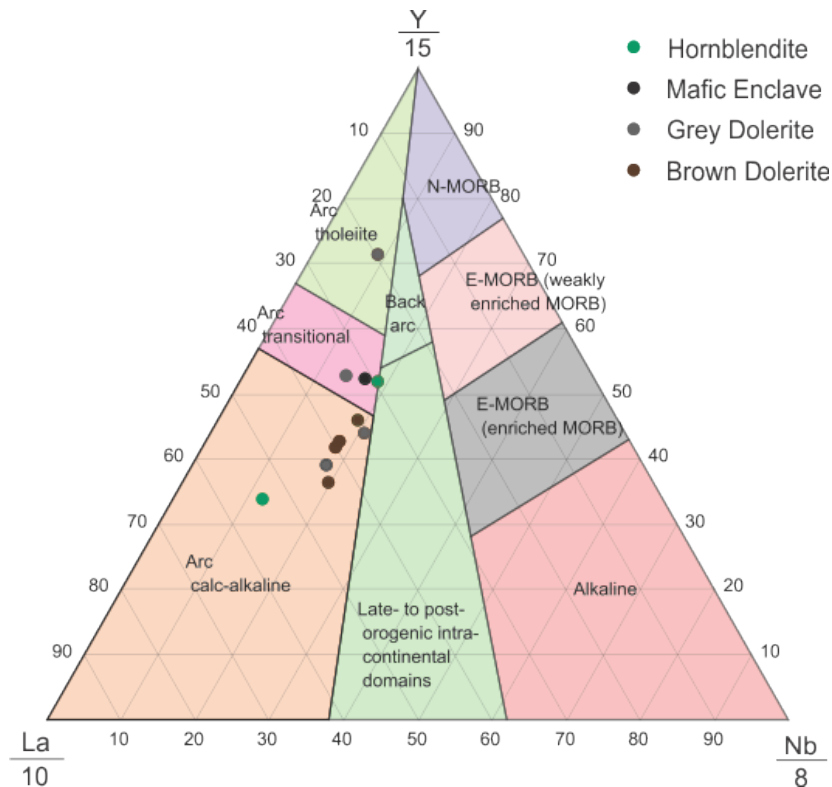
Figure 18: Basalt tectonic classification diagram (Cabanis and Lecolle, 1989). Samples plotted by Y/15, La/10 and Nb/8.

36
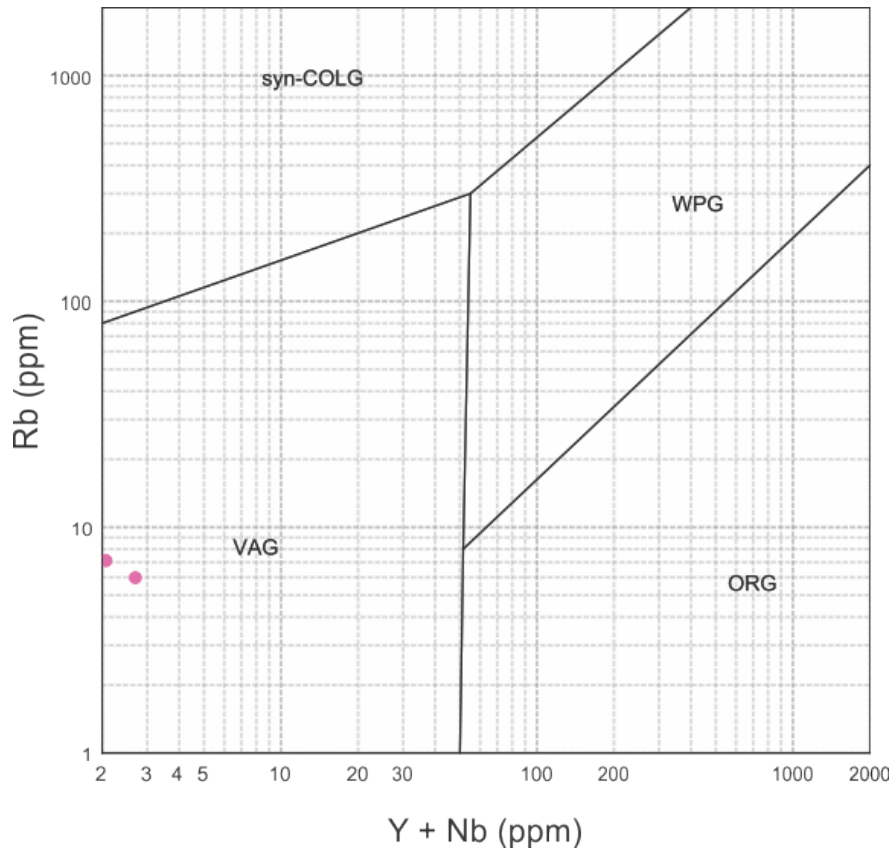
Figure 19: Tectonic classification diagram for granite. Y+Nb on the x-axis and Rb on the y-axis (Pearce et al. 1984). The fields displayed are "syn-collisional granites", "within-plate granites", "ocean-ridge granites" and "volcanic arc granites".
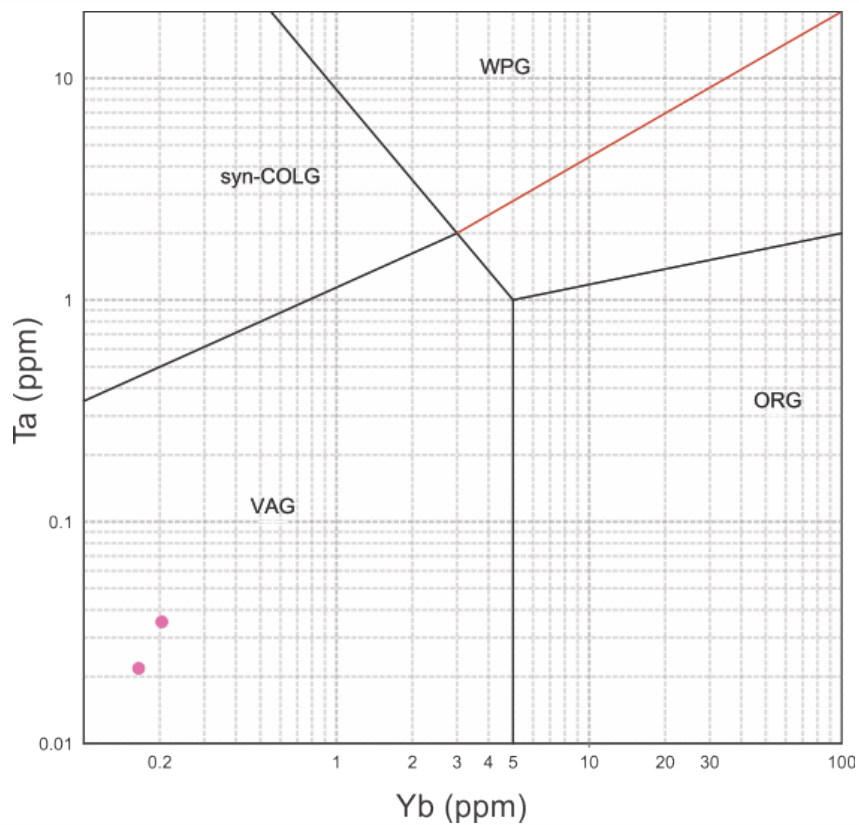
Figure 20: A granite tectonic classification diagram with Yb on the x-axis and Ta on the y-axis (Pearce et al. 1984). Classification fields are the same as figure 19.

37

DISCUSSION

Age and Origin of the Jebel Ja'alan Igneous Intrusive Suite

GRANITE

The zircon data from O14-37 and JA15-33 yield poorly defined ages of 843 ± 20 Ma (figures 5 and 6) and 835 ± 35 Ma respectively (figures 8 and 9). These correlate well with a 850 ± 27 Ma Rb-Sr whole-rock isochron age from Gass et al. (1990) on the Jebel Ja'alan suite. However, most of the analysed zircons were very discordant and were evidently heavily affected by common lead, so these data should be treated as a vague indicator only.

The granite samples JA15-33 and O14-37 gave positive εHf values between +2.30 and +10.17 (figure 11 and table 1), indicating the batholith originates from a juvenile mantle source. The sample JA15-18 was analysed for Sm-Nd and also returned a positive ε value of +1.72 (figure 12 and table 2). The Hf depleted mantle model ages ranged between 990 Ma and 1220 Ma with an average of 1130 Ma, while the Nd model age yielded a slightly older date of 1291 Ma. This slight discrepancy might reflect the relative timing of growth of the zircon, early in the cooling history, whereas the Nd model age reflects the whole rock. This whole rock composition may reflect the consumption of more country rock than the early-formed rock.

Figure 15 shows the granite lines quite flat in shape but there is an overall decrease in enrichment compared to the average chondrite line with increasing atomic number. Volcanic arc granites have this pattern because the light REE are soluble in subduction-derived fluids and will therefore be enriched in subduction-related igneous rocks. On

tectonic classification diagrams by Pearce et al. (1984) (figures 19 and 20), the samples were placed in the volcanic arc fields due to their low concentrations in the HFS elements Y, Nb, Ta and Y which are found in low concentrations in volcanic arc magmatism. This is because the HFSE are not readily soluble in the fluids produced during the dehydration of subducted oceanic crust and therefore calc-alkaline granites contain low concentrations of HFSE. Therefore the trace element data shown in the REE spider plots and granite tectonic discrimination diagrams conclusively show the Ja'alan Granite to be of island arc affinity.

DYKE SWARM

Three separate lithologies make up the dyke swarm of Jebel Ja'alan: an early dolerite, an andesite and a late dolerite. Each dyke type is temporally distinct and shows clear cross-cutting relationships for their relative timing. The εNd values of the dykes were all positive and plotted between the depleted mantle and CHUR line, this suggests that the dyke swarm has a juvenile mantle origin like the granite. With decreasing age, the separate dyke generations decrease in juvenility, where the first dolerite is the most juvenile (εNd = +6.78), followed by the andesite (+4.32) and then the second dolerite as the most magmatically evolved (+0.56) (table 2).The depleted mantle model ages for all generations were derived from Sm-Nd data and were older than the DM model age of the granite. From field data these model ages do not simply fit the cross-cutting relationships, as it is expected that the model ages would decrease in age from the granite to the late dolerite. However, Elburg and Foden (1998) provided evidence from Sulawesi, Indonesia that $^{143}Nd/^{144}Nd$ variations can show a changing magma evolution due to variation in the magma source (i.e. mantle wedge and subducting slab). Thus with this suite of Nd data, the model ages may have been distorted by the progressive

assimilation of older sediment off the subducting slab into the mantle wedge, thus significantly contaminating the lithospheric mantle beneath the Ja'alan arc terrane. The decreasing juvenility in the dyke generations supports this idea of progressive sediment contamination in the mantle wedge. When crustal extension took place post-orogenesis, the intruding dykes may then have been sourced from the underlying lithospheric mantle. The other possible reason for the anomalously older model ages is that the dykes melted and assimilated basement gneisses and schists. A similar situation was found in the Saudi Arabian terranes where the younger eastern arc terranes have older Nd model ages than the older western arc terranes (Stoeser and Frost 2006).

Worthing (2005) suggests that, similar to other extensional areas, the dyke swarm of Mirbat was formed by melting of the subduction altered lithospheric mantle and emplaced by crustal extension. This interpretation is supported in Jebel Ja'alan. Due to the ubiquity of geochemical signatures in dykes of the ANS it could be possible that such a modified mantle is regionally developed (Worthing 2005).

Figure 15 shows the two dolerites to have shallow curves but there is still a decrease in element enrichment with increasing atomic number. The andesites show the same relationship between atomic number and relative enrichment but with a steeper angle than the dolerites. Petrological and field interpretation of the brown dolerite is at odds with an island arc setting, as the presence of the alkaline minerals sanidine and nepheline, combined with the thickness and steepness of the dykes made for strong evidence of an extensional setting following accretion. Further to this, basalt tectonic classification diagrams plot the dyke samples in the volcanic arc basalt calc-alkaline

basalt and volcanic arc basalt island arc tholeiite. The dykes therefore display island-arc geochemistry but the tectonic setting of the later generation was likely extensional and thus probably had relict geochemistry from the subduction-altered lithospheric mantle.

Regional Tectonic Setting of Jebel Ja'alan

The results suggest that the basement formed a juvenile, calc-alkaline island arc. This island arc would have been located in a Neoproterozoic ocean prior to its final closure. More specifically, the igneous suite of Jebel Ja'alan is related to the closure of the Mozambique Ocean during Gondwana assembly. This is supported by recent studies of the ANS purporting it to be an accretion of intra-oceanic island arcs from the Mozambique Ocean (Johnson et al. 2011, Collins and Pisarevsky 2005, Meert 2003, Cox et al. 2012, Johnson and Woldehaimanot 2003). Because Ja'alan shows no evidence of metamorphism after ~830 Ma (Alessio 2015), it was likely already accreted to other terranes at this time, long before final accretion of the ANS.

The Sm-Nd data for the dyke swarm consistently show a juvenile nature with little or no interaction between the mantle and the crust similar to Robinson et al. (2014). The island arc magmatism seen at Jebel Ja'alan is relatively coeval with the island arc magmatism from Saudi Arabia (~850 Ma, Robinson et al. 2014) and the Sadh gneiss complex of Mirbat (831 ± 7 Ma and 835 ± 6 Ma, Rantakokko et al. 2014), as well as the granodioritic basement of Al Jobah (821 – 836 Ma, Bowring et al. 2007) and some zircons from the volcanics in Jebel Akhdar (812 - 829 Ma, Bowring et al. 2007) although Jobah and Akhdar are likely slightly younger. Stoeser and Frost (2006) showed that the Neoproterozoic terranes of Saudi Arabia can be divided into western arc terranes (870 - 800 Ma), eastern arc terranes (620 - 740 Ma) and the Khida terrane

(>1660 Ma) (figure 21). The Ja'alan Granite is similar in age to the granites of the western arc terranes but has a εNd value more similar to the eastern arc terranes where the values range from 0.0 to +3.9. This suggests that the Midyan, Hijaz, Jiddah and Bidah terranes (figure 21) were crystallising relatively coevally above a subduction zone on the opposing margin of the Mozambique Ocean to Jebel Ja'alan. However the parent melt responsible for the Jebel Ja'alan pluton was probably slightly more contaminated with crustal rock than its western arc terrane counterparts, as seen through εNd data.

Despite some similarities in the ages of intrusions, Jebel Ja'alan differs from Mirbat and the Saudi terranes in many ways. Granitic magmatism in Saudi Arabia is long-lived (~845 Ma to ~525 Ma) and has been used to define discrete magmatic events in the ANS (Robinson et al. 2014). In Mirbat, granitic magmatism is also present for a much greater time span than in Jebel Ja'alan, lasting from >850 Ma to 726 Ma (Rantakokko et al. 2014, Bowring et al. 2007, Mercolli et al. 2006). The metamorphic history of Mirbat is also much longer, with the region undergoing deformation events at *ca.* 815-820 Ma, *ca.* 790-800 Ma and *ca.* 718 Ma (Rantakokko et al. 2014). In comparison, Jebel Ja'alan has only one major granitic magma event at ~840 Ma and one deformation event at ~830 Ma.
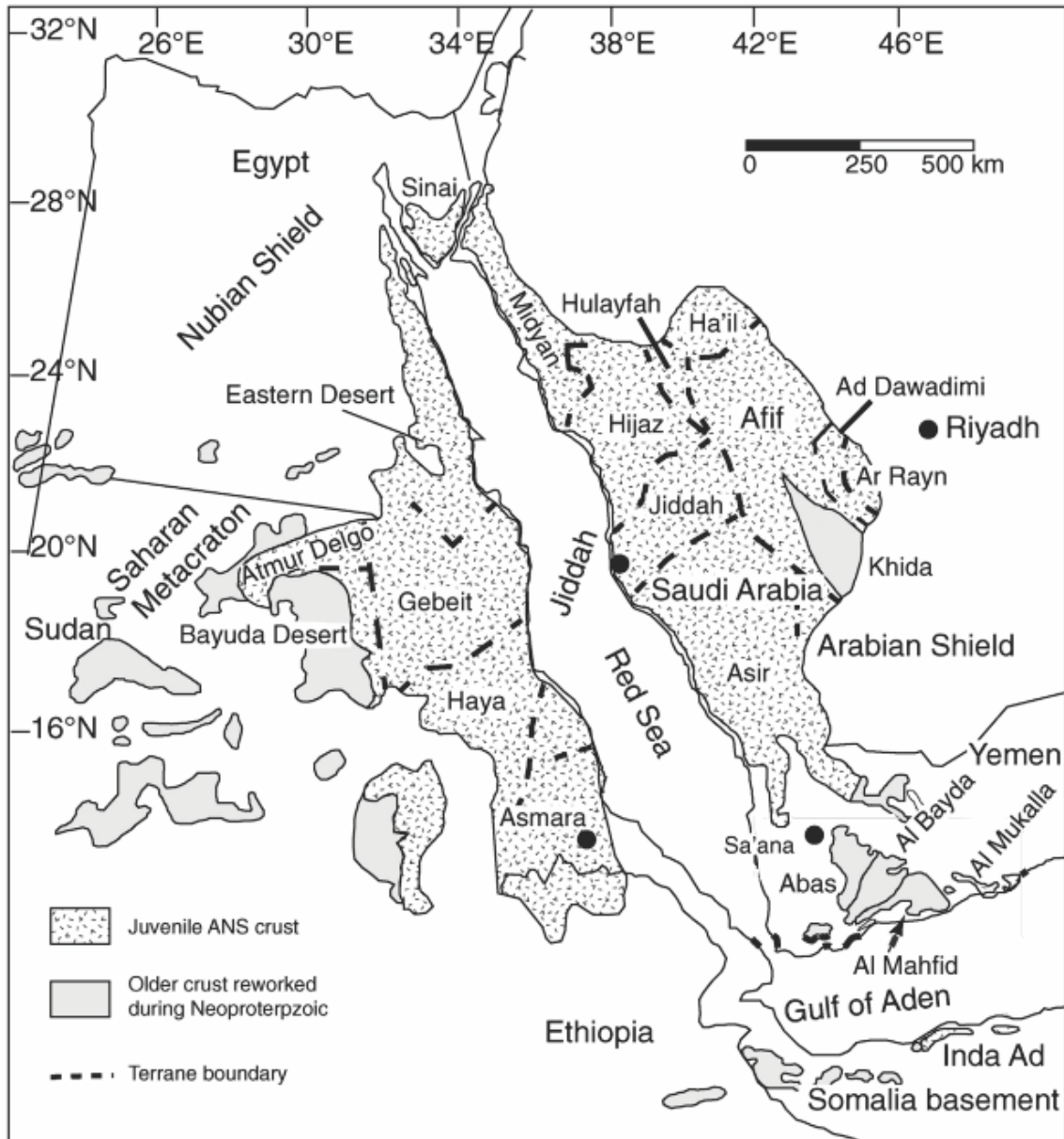
Figure 21: Map showing the terranes of the ANS across north-eastern Africa and the western Arabian Peninsula. The speckled areas are juvenile crust and plain grey areas are older reworked crust (modified from Yeshanew et al. 2015).

Like Jebel Ja'alan, Mirbat also has a major NW-SE trending dyke swarm, which has been shown to be ~700 Ma (Worthing 2005). This dyke swarm also has a geochemical signature that suggests an island arc setting. As well as this, Gass et al. (1990) reported a K/Ar date of 604 ± 24 Ma from a mafic dyke in the Mirbat region, and an $^{39}Ar/^{40}Ar$ plateau age of 617 ± 3.5 Ma from a mafic dyke on the Hallaniyat Islands. Ba-Bttat (1991) reported a hornblende $^{40}Ar/^{39}Ar$ date of 693 ± 12 Ma and 585 ± 11 Ma for two dyke generations in the Al Bayda terrane of Yemen. The above ages show two distinct age groupings (~700 Ma and ~600 Ma) and are possibly repeated in Jebel Ja'alan, however without crystallisation ages we cannot know definitively. Worthing (2005) interpreted the ~700 Ma NW-SE dyke generation to have been emplaced in conjugate strike-slip fractures resulting from regional E-W compression either during the strike-slip movements or in later extensional movements. While the ~600 Ma second phase generation was emplaced in a regional extensional collapse. Because of the pervasive source of these movements (i.e. the formation of Gondwana), it is reasonable to use this interpretation on the dyke swarm of Jebel Ja'alan. On the far side of the Arabian Shield in the Sinai Peninsula, the basement is also cross-cut by a remarkable dyke swarm (El-Sayed 2006). Trace element geochemistry here shows the swarm to be calc-alkaline, while field observations show that it was emplaced in an extensional, post-subduction setting. This is strongly similar to the dyke swarm presented here, over 2500 km east of Sinai, and is a further testament for the continent-scale tectonic forces that would have been pervading the ANS during Gondwana formation.

CONCLUSIONS

A calc-alkaline batholith of granite located in Jebel Ja'alan, NE Oman, was emplaced in the basement gneisses and schists of an intra-oceanic arc of the Mozambique Ocean.

The island arc was likely located close to the margin of Neoproterozoic India. U-Pb geochronology suggests that the granite pluton was emplaced at ~840 Ma and with the lack of metamorphism seen in the Ja'alan Granite, accretion must have occurred before crystallisation. The rare earth elements of the samples normalised to the chondritic average shows characteristic patterns for a calc-alkaline parent magma. Tectonic classification diagrams using trace element data provide the evidence for an island arc setting. Nd and Hf analyses provide ε values from +0.56 to +6.78 and +2.30 to +10.17 respectively. These suggest a juvenile mantle origin for the rocks with little or no crustal interference. Depleted mantle model ages from Sm-Nd data show evolved Mesoproterozoic ages for the dyke swarm between 1309 Ma and 1663 Ma that suggest subduction-related contamination of the underlying lithospheric mantle during ocean closure. Similarities between the dyke swarms of Saudi Arabia, Yemen and Mirbat to Jebel Ja'alan suggest that they were emplaced following E-W compression, which formed conjugate NW-SE strike slip fractures. The dykes may have been emplaced in these fractures during the strike-slip movement and later extensional collapse of the shield.

REFERENCES

ALESSIO B. 2015 The Structural and Metamorphic Evolution of the Neoproterozoic Basement in Jebel Ja'alan, East Oman. Department of Geology and Geophysics. University of Adelaide.

ALLEN P. A. 2007 The Huqf Supergroup of Oman: Basin development and context for Neoproterozoic glaciation, *Earth-Science Reviews,* vol. 84, pp. 139-185.

ALLEN P. A., LEATHER J. & BRASIER M. D. 2004 The Neoproterozoic Fiq Glaciation and its Aftermath, Huqf Supergroup of Oman, *Basin Research,* vol. 16, pp. 507-534.

ALLEN P. A., *et al.* 2011 The Abu Mahara Group (Ghubrah and Fiq formations), Jabal Akhdar, Oman, *Geological Society, London, Memoirs,* vol. 36, pp. 251-262.

BA-BTTAT M. A. O. 1991 Geology, petrochemistry and tectonics of the Lowder-Mudiah area, Abyan Province, Yemen Republic. Ann Arbor: University of Leicester (United Kingdom).

BOWRING S. A., *et al.* 2007 Geochronologic Constraints on the Chronostratigraphic Framework of the Neoproterozoic Huqf Supergroup, Sultanate of Oman, *American Journal of Science,* vol. 307, pp. 1097-1145.

BOWRING S. A. & MARTIN M. W. 1999 High precision U-Pb geochronology, the tempo of evolutionand the record from Gondwana, *Journal of African Earth Sciences,* vol. 28, no. 1, pp. 187-201.

BOYNTON W. V. 1984 Chapter 3 - Cosmochemistry of the Rare Earth Elements: Meteorite Studies, *Rare Earth Element Geochemistry,* vol. 2, pp. 63-114.

CABANIS B. & LECOLLE M. 1989 Le diagramme La/10-Y/15-Nb/8: un outil pour la discrimination des series volcaniques et la mise en evidence des processus de melange et/ ou de contamination crustale, l'*Academie des Sciences Series II,* vol. 309, pp. 2023-2029.

CHALK H. C. 2014 Mesoproterozoic Bimodal Magmatism of Southern Australia: Assessing Relative Mantle Input and Implications for IOCG Mineralistion Prospectivity. Department of Geology and Geophysics. pp. 67. Adelaide: University of Adelaide.

COLLINS A. S. & PISAREVSKY S. A. 2005 Amalgamating eastern Gondwana: The evolution of the Circum-Indian Orogens, *Earth-Science Reviews,* vol. 71, no. 3–4, pp. 229-270.

CORFU F., *et al.* 2003 Atlas of Zircon Textures, *Reviews in Mineralogy and Geochemistry,* vol. 53, no. 1, pp. 469-500.

COX G. M., *et al.* 2012 Ediacaran terrane accretion within the Arabian–Nubian Shield, *Gondwana Research,* vol. 21, pp. 341-352.

DE LA ROCHE H., *et al.* 1980 A Classification of Volcanic and Plutonic Rocks using R1-R2 Diagrams and Major Element Analyses - its Relationship and Current Nomenclature, *Chemical Geology,* vol. 29, pp. 183-210.

EL-SAYED M. M. 2006 Geochemistry and petrogenesis of the post-orogenic bimodal dyke swarms in NW Sinai, Egypt: constraints on the magmatic–tectonic processes during the late Precambrian, *Chemie der Erde - Geochemistry,* vol. 66, no. 2, pp. 129-141.

ELBURG M. & FODEN J. 1998 Temporal changes in arc magma geochemistry, northern Sulawesi, Indonesia, *Earth and Planetary Science Letters,* vol. 163, no. 1–4, pp. 381-398.

FAURE G. & MENSING T. M. 2005 Isotopes: Principles and Applications*.* (3rd edition). John Wiley & Sons, Inc, Hoboken, New Jersey.

GASS I. G.*, et al.* 1990 Tectonics, geochronology and geochemistry of the Precambrian rocks of Oman, *Geological Society Special Publication,* vol. 49, no. The Geology and Tectonics of the Oman Region pp. 585-599.

JOHNSON P. R. 2003 Post-amalgamation basins of the NE Arabian shield and implications for Neoproterozoic III tectonism in the northern East African orogen, *Precambrian Research,* vol. 123, no. 2–4, pp. 321-337.

JOHNSON P. R.*, et al.* 2011 Late Cryogenian–Ediacaran history of the Arabian–Nubian Shield: A review of depositional, plutonic, structural, and tectonic events in the closing stages of the northern East African Orogen, *Journal of African Earth Sciences,* vol. 61, pp. 167-232.

JOHNSON P. R. & WOLDEHAIMANOT B. 2003 Development of the Arabian-Nubian Shield: Perspectives on Accretion and Deformation in the Northern East African Orogen and the Assembly of Gondwana, *Geological Society, London, Special Publications,* vol. 206, pp. 289-325.

KIL Y. & JUNG H. 2015 LA-ICP-MS analysis of natural rock samples using XRF glass beads, *Geosciences Journal,* vol. 19, no. 1, pp. 45-52.

LEATHER J.*, et al.* 2002 Neoproterozoic snowball Earth under scrutiny: Evidence from the Fiq glaciation of Oman, *Geology,* vol. 30, no. 10, pp. 891-894.

MEERT J. G. 2003 A synopsis of events related to the assembly of eastern Gondwana, *Tectonophysics,* vol. 362, pp. 1-40.

MEERT J. G. & LIEBERMAN B. S. 2007 The Neoproterozoic assembly of Gondwana and its relationship to the Ediacaran–Cambrian radiation, *Gondwana Research,* vol. 203, pp. 1-17.

MEERT J. G. & VAN DER VOO R. 1997 The assembly of Gondwana 800-550 Ma, *Journal of Geodynamics,* vol. 23, no. 3–4, pp. 223-235.

MERCOLLI I.*, et al.* 2006 Lithostratigraphy and geochronology of the Neoproterozoic crystalline basement of Salalah, Dhofar, Sultanate of Oman, *Precambrian Research,* vol. 145, pp. 182-206.

MIDDLEMOST E. A. K. 1994 Naming Materials in the Magma/Igneous Rock System, *Earth Science Reviews,* vol. 37, pp. 215-224.

PEARCE J. A. & CANN J. R. 1973 Tectonic Setting of Basic Volcanic Rocks Determined Using Trace Element Analyses, *Earth and Planetary Science Letters,* vol. 19, pp. 290-300.

PEARCE J. A., HARRIS N. B. W. & TINDLE A. G. 1984 Trace Element Discrimination Diagrams for the Tectonic Interpretation of Granitic Rocks, *Journal of Petrology,* vol. 25, pp. 956-983.

RANTAKOKKO N. E.*, et al.* 2014 Neoproterozoic evolution of the eastern Arabian basement based on a refined geochronology of the Marbat region, Sultanate of Oman, *Geological Society, London, Special Publications,* vol. 392, pp. 107-127.

ROBINSON F. A., *et al.* 2014 Arabian Shield magmatic cycles and their relationship with Gondwana assembly: Insights from zircon U–Pb and Hf isotopes, *Earth and Planetary Science Letters,* vol. 408, pp. 207-225.

ROGERS J. J. W., UNRUG R. & SULTAN M. 1995 Tectonic assembly of Gondwana, *Journal of Geodynamics,* vol. 19, no. 1, pp. 1-34.

ROLLINSON H. 1993 Using Geochemical Data: Evaluation, Presentation, Interpretation. Routledge, New York, USA.

STOESER D. B. & FROST C. D. 2006 Nd, Pb, Sr, and O isotopic characterization of Saudi Arabian Shield terranes, *Chemical Geology,* vol. 226, no. 3–4, pp. 163-188.

WOOD D. A. 1980 The Application of a Th-Hf-Ta Diagram to Problems of Tectonomagmatic Classification and to Establishing the Nature of Crustal Contamination of Basaltic Lavas of the BritishTertiary Volcanic Province, *Earth and Planetary Science Letters,* vol. 50, pp. 11-30.

WORTHING M. A. 2005 Petrology and geochronology of a Neoproterozoic dyke swarm from Marbat, South Oman, *Journal of African Earth Sciences,* vol. 41, no. 3, pp. 248-265.

YESHANEW F. G., *et al.* 2015 Zircon U–Pb geochronology and Nd isotope systematics of the Abas terrane, Yemen: Implications for Neoproterozoic crust reworking events, *Precambrian Research,* vol. 267, pp. 106-120.

APPENDIX A: METHODOLOGY

Mineral Separation and Geochemistry Sample Preparation

CRUSHING

1. Cut the rocks using the rock saw (room B21d of Mawson Laboratories at the University of Adelaide).
2. Make sure that the rocks are dry, clean and fresh. Ensuring that there is no lichen or texta left on the rocks.
3. Clean the jaw crusher (room B21a) before and after use using compressed air and ethanol.
4. Line the tray with butcher paper to ensure that the samples are not contaminated.
5. The disc mill (room B21a) is used to achieve the zircon fraction. Clean the machine using compressed air and ethanol.
6. Move the discs until the desired gap is reached. Start at 1mm.
7. Run this through the sieve using <79 μm and >479 μm mesh. Place the sieve into the Endcotts EPL2000 Super Shaker and allow time for the fractions to separate.
8. Take the course fraction >479 μm and run it through the disc mill again, changing the spacing between the discs to 0.7mm.
9. Repeat this process again with the spacing at 0.4mm.
10. Put each fraction into the sample bags. Labelling '>479 μm', 'Zircon fraction' and '<79 μm'

11. If samples are undergoing geochemistry, after they have been through the jaw crusher they are placed into the ring mill (room B21a) using the tungsten carbide container and rings. The ring mill is cleaned with compressed air and ethanol.
12. Quartz blank is first used to ensure contamination is kept at a minimum. The quartz is run for 1.5 minutes.
13. The samples are then placed into the tungsten carbide mill and run for 3 minutes.
14. This fraction is then placed in a sample bag for later use.
15. Zircon Separation
16. The separation was done in the Mawson Building lab B29d at the University of Adelaide.
17. The room is cleaned before each use. The benches are cleaned and the room is vacuumed.
18. The sample is panned removing the lights from the fraction. The lights are placed into a funnel with filter paper and later dried in the oven.
19. The heavies extracted by this method are then placed on the hotplate to dry at 50 °C. To separate the magnetic material the sample is put through the Frantz machine.
20. For the first time the sample is run through at 0.5 amps. This will separate the highly magnetic minerals. This is repeated two more times. The magnet is turned up to 1 amps and 1.7 amps respectively. Each magnetic fraction is placed in a sample bag and clearly labelled.

HEAVY LIQUIDS

Funnel lined with filter paper

Burette with Methyl Iodide filled to the line

Funnel lined with filter paper

Funnel lined with filter paper

Conical Flask
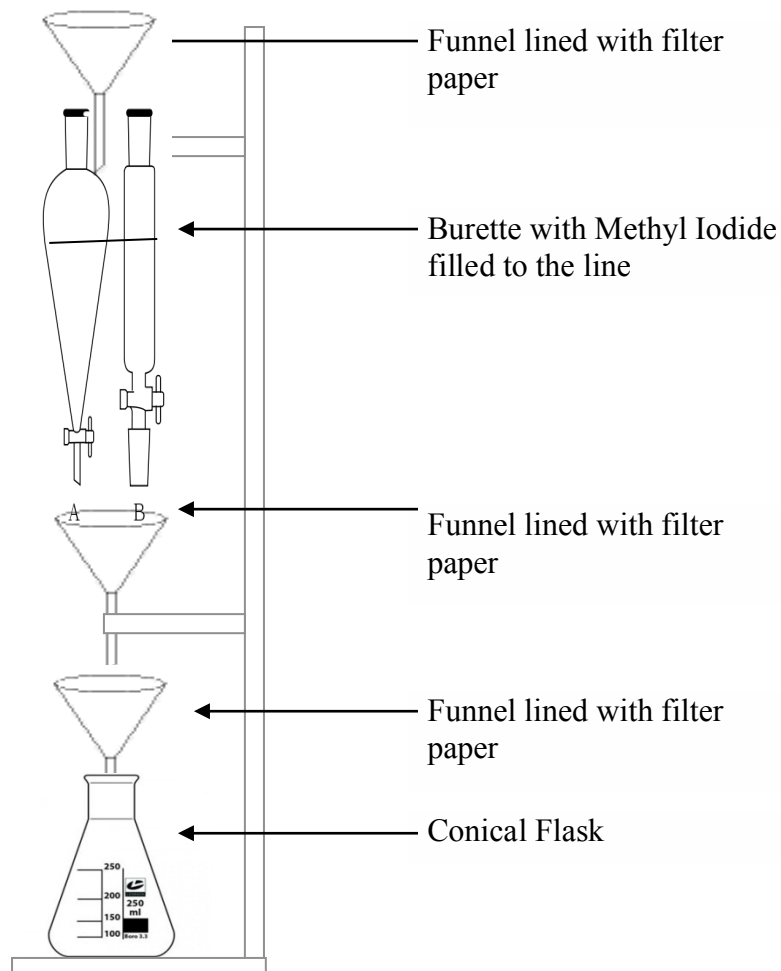
Figure 22: The set up for the separation of zircons via the use of heavy liquids.

Fill the burette with methyl iodide. The methyl Iodide allows for the zircons to sink to the bottom. Take the top funnel off and poor the remaining fraction of the sample into the separating funnel (burette). Stir it with a stirring rod and allow for the separates to drop to the bottom. Tap off and stir again. This needs to be repeated until there are no more particles sinking. Everything that the heavy liquid touches has to be cleaned 10 times with ethanol. The zircons are then dried on a hot plate with a funnel over the top to stop any from blowing away. The separates remaining are cleaned, dried and placed into a sample bag.

ZIRCON MOUNTING

The zircons were hand-picked under an Olympus SZ51 microscope (room G36) and stuck to tape on a plastic slide. Using a mould, epoxy resin was poured onto the picked zircons and left to set for 24 hours. Once set, the mount was removed from the mould and the slide with which the picked zircons were placed on. The mount was then grinded down to size using the Knuth Rotor machine (room B21d). Following this, the mount was polished, using a Selbys Scientific Ltd DP-U4 polishing machine and polish sprays (room B21d) to expose the minerals and then it was sent to Adelaide Microscopy to be carbon coated.

Thin Sections

1. 10 samples were sent to Continental Instruments, Lucknow, India. Thin-sections were made polished and uncovered. The following method was used.
2. First, a small slab is cut, approximately 25mm x 55mm, x 8mm thick, using a 250mm diameter rock-cutting saw blade with a continuous diamond rim.
3. A top surface on the slab, is manually ground flat on a bench-mounted, horizontal diamond grinding wheel Habit-brand, grit size 64.
4. The coarse ground top surface is warmed on a hot plate (at $50^{\circ}C$), and the top coarse-ground surface is impregnated with an epoxy mix of Araldite LC191 resin, with HY951 hardener, ratio 8:1. This surface is then manually more finely ground flat using 600 SiC grit, on a zinc-lap or glass plate, using water as a lubricant. This flat finely ground surface is cleaned, checked manually for "perfection", (if open porosity is still exposed another veneer of epoxy is applied), is then glued onto a clean, dry glass slide, ground to a known thickness, using a UV curing, cyanoacrylate liquid adhesive "Loctite Impruv 36331". [Exposure to a UV light of the glued interface through the back of the glass slide cures the adhesive in 2 to 3 minutes. This is a permanent bond, and the rock (or eventual wafer) cannot be ever separated from the glass.
5. The block mounted on glass is then cut off using a trim saw with a thin continuous diamond rimmed sawblade (Diatrenn E2-G), to leave a thickness of about 1mm of the sample slab (glued onto the glass slide), with the top surface exposed for further processing.

6. The 1mm slab thickness is further ground down on a diamond wheel (Habit D76) held within a special jig attachment by vacuum, using water as a lubricant. This reduces the slab thickness stuck on the glass, to a wafer of about 120 micron (0.12mm).

7. The glass slide of known thickness with the glued-on rock wafer is then loaded and held in place on the face of a special jig, and lapped flat on a Logitech machine, to a final petrographic thickness of the rock wafer, of 30 micron, using 600 SiC grit as the grinding abrasive, and water as a lubricant.

8. When the Logitech lapping cycle is finished, the quality of the wafer on the glass is assessed, also optically checked for the required 30 micron thickness, and when confirmed as correct, the section is cleaned and covered with a glass coverslip, using the same UV curing adhesive as listed above. Again this is a permanent fix, i.e. the coverslip cannot be removed. The final thin section is then again cleaned and labelled.

SEM Imaging

Machine used: Philips XL20 SEM with EDAX EDS and Gatan Cathodoluminescence (CL) detector (Waite Campus, University of Adelaide)

LOADING A SAMPLE

1. To place a sample into the microprobe: Open the SEM viewing application on the right-hand desktop (first-time users will have to create a username and password).

2. Check that the microprobe is set on SE and the beam is turned off by clicking the kA button on the far right of the screen.

3. Now vent the vacuum chamber by pressing the 'Vent' button next to the kA button. You will hear the chamber being vented.

4. The door on the chamber will not open automatically after venting is complete, so after approximately two minutes try gently pulling on the black door handle.

5. Using gloves, the zircon mount must be placed in a hollowed-out holder. Check that the top surface of your mount is completely flat to the top surface of the holder.

6. Turn screw on the side of holder using an alan key to make sure mount is held firmly in place. Thin black tape is provided in the SEM XL20 room, this should be taped to the top and bottom edges of the mount and round the sides of the holder, taking care not to tape over any zircons.

7. Screw the sample holder into the screw hole on the door of chamber.

8. To check that the sample fits into the chamber, turn the blue knob on the exterior of the machine anticlockwise to bring the arm of the CL detector into the chamber. Carefully begin to close the door, while looking to see if the mount holder will collide with the Cl detector. If the sample touches the detector, then retract the detector by turning the blue knob clockwise and lower the holder.

9. If the sample clears the detector and the door can be shut with no resistance, retract the detector and close the door of the chamber.

10. Keeping the door closed with your hand, press the 'pump' button in the microprobe application to pump the chamber. Once pumping is complete, the sample is ready to be analysed.

IMAGING

1. To view the zircon samples, turn the beam on in the beam menu by clicking the 'kA' button.
2. Set the beam to backscatter by selecting BSE under the 'detectors' tab. Set the spot size to 5 and the kA value to 20 under the 'beam' tab.
3. Navigate your mount using the mouse. The mouse can be used to track in any direction, focus the image and zoom.
4. To reduce the noise and increase the resolution of the image, the scanning speed can be adjusted under the 'scan' tab, however this comes at the cost of slower updating of the display and slower tracking across mount. Thus it is recommended that 'slow scan speed 1' is used when tracking, 'slow scan speed 2' is used when improving the image quality and 'slow scan speed 3' is used for image capture.
5. Capture images of the zircons by selecting 'image' under the 'in/out' tab. Create a folder and save each image there with an easily identifiable name.
6. Once the entire sample has been imaged, proceed to analyse sample under CL.
7. Insert CL detector into chamber by turning blue knob anticlockwise. The screen will go black as the detector comes under the beam. Slowly continue to turn blue knob until sample image reappears onscreen.
8. Now change the beam to CL by selecting 'IMG' under the 'detectors' tab. Change the spot size to 7 and the kA value to 12 under the 'beam' tab. Adjust the contrast and brightness on the monitor to improve image. Increase magnification to ensure that zircon zoning is discernible.
9. When using CL, the image can be further improved using the control box situated between the two monitor screens. The far left knob controls the kV, this should be increased to 500. Next to this are the brightness and contrast knobs that can be used to further optimise the image.
10. Images are captured in the same way as explained for backscatter images. Name the CL files so they can be distinguished from the BSE images.
11. When imaging is complete, make sure the CL detector is fully retracted, change the beam back to SE and turn the beam off. The chamber can now be vented. When chamber is fully vented, open the chamber door and, using gloves, remove the mount and holder. Remove mount from holder and place holder back in the box next to SEM.

LA-ICP-MS (U-Pb)

U-Pb zircon dates were obtained using a New Wave UP-213 laser attached to an Agilent 7500x ICP-MS. The following method from Adelaide Microscopy was used to obtain U-Pb data from zircons:

TURNING ON THE GASES AND INSERTING SAMPLES

1. Ensure ICP-MS is in standby mode.
2. Start ICP-MS top program and select the tune menu from the 'instrument' menu.
3. Loosen the screws on the laser ablation chamber door and slide the door to the left. The sample holder will then slide out.
4. Clean your samples and place them in the cell, ensuring they are held tightly.
5. Insert the cell into the chamber, close the door and tighten the screws.
6. Start ICP-MS top program (middle computer).
7. Select 'instrument control' from the instrument menu.
8. Select 'maintenance menu' then 'sample introduction'.
9. Check box 'optional gas' and type 60% for 'optional gas' and click on enter.
10. Open 'laser ablation' program on the New Wave computer (far right computer).
11. Click on 'evacuate' a dialogue box will pop up with a status bar, indicating number of cycles. The laser ablation chamber and then refilled with He in cycles.
12. Once finished click on 'evacuate' twice more. The system needs to do 30 cycles to remove all the air from the chamber.
13. Once finished ensure 'online is selected in the laser ablation program.
14. Close 'sample introduction' dialogue in the ICP-MS top program. This action will reset the optional gas to 0%

TURNING ON THE PLASMA

1. Select instrument > tune.
2. Select 'optional gas' slider bar (probably set at around 58%) and turn it down to 20%.
3. Select instrument > instrument control.
4. Select instrument > instrument control > start plasma.
5. Wait until the plasma is fully operational (all gauges green, approximately 2 minutes).
6. Go back to instrument > tune and turn optional gas back up to correct value (usually 58-59%).
7. Perform a maintenance log by carrying out the following steps:
    a. On the 'instrument control' screen select the 'diagnostics log' menu and then 'log book'.
    b. Make a note of the 'plasma on' time, then exit.
    c. On the 'Instrument control' screen select the 'maintenance log' menu then 'log book'.
    d. Double click on one of the previous logs, select and copy the information in the 'comments' box. Click close.
    e. Click 'record log' and paste copied data into the 'comments' box, then add in today's details including the 'plasma on' time you made a note of.
    f. Click 'ok' then 'exit'.
8. Select instrument > tune

LOAD METHOD

1. On the Chemstation computer select the methods menu, load.
2. For example select BenZirc.M for zircon dating, or BenMnz.M for monazite dating, etc and click ok.
3. Choose the equivalent calibration file (with a C extension) and click ok.
4. In laser ablation mode (compared to solution ICP-MS) the calibration file is not used however the software will still require this file, if no equivalent calibration file can be found then select Default.C

PA FACTOR

The PA factor allows the ICP-MS software to process signals acquired by the detector in pulse count mode and analogue mode with seamless/linear calibration. This transition in the way the signal is measured occurs when counts per second exceed approximately one million. Thus the PA factor is not required every time the system is run, only when you expect cps to exceed approximately one million in your unknown (note: always perform a PA factor if attempting geochronology, as counts in zircon and monazite typically exceed one million). When conducting a PA factor what we are attempting to do is trip the detector into analogue counting mode by obtaining over a million counts in at least two elements at opposite ends of the mass spectrum you are analysing. We do this by increasing the spot size and intensity of the laser, and ablate a high concentration NIST glass.

1. Move to Nist 610 (High concentration NIST, dark blue glass).
2. Initially, change the beam to 65 μm and increase frequency to 10Hz.
3. To view the counts on the detector of specific isotopes click on the 'Acq. Params' menu, acquisition parameters, and tick 80, 206, 248/232, 207, 208, 204, 238, 220, click ok. These isotopes will now appear on the tune screen.
4. Start laser firing, click start on the tune screen.
5. When over one million counts in ^{238}U and ^{208}Pb click stop on the tune panel, select tune > P/A factor > click 'load masses from Acq. Method' > run. (Note: If unable to obtain over one million counts, try an 80 μm beam diameter. If sensitivity continues to be too low, try increasing the beam intensity).
6. When the notepad automatically pops up, check that ^{238}U and ^{208}Pb are in detection range (they will have a number next to them, usually about 0.9), then click 'yes' to a new P/A factor, click save. (Note: if there are no numbers next to any of the masses, and you did have over a million counts in the tune screen, it could be that you didn't perform step 5 fast enough and the counts dropped below a million. Simply repeat step 5).
7. Stop laser firing, close shutter.
8. Turn the settings back to normal, 5Hz for laser fire rate, and 15 μm (monazite) or 30-50 μm (zircon) for spot size and 65% intensity.

SETTING UP THE LASER ABLATION SYSTEM

1. Open 'laser ablation' program on the New Wave computer.
2. Turn up light intensity and choose COAX mode of sample illumination.

3. Choose 5Hz for laser fire frequency/rate.
4. Select a laser spot size dependent on your method of analysis (e.g 8-15 µm for monazite, 30 µm for zircon).
5. Select a power rating (e.g. 70-80% for monazite, 60-80% for zircon). This value is a percentage of the maximum power available, and the value you choose will be dependent on your required spot size and concentration of elements of interest in your sample. Ask an AM staff member if unsure.
6. In order to view the sample surface, the user can adjust the optical zoom. To locate samples use a zero value for the optical zoom, when using the laser increase this zoom to 50% (zircon or thin sections) or 75% (monazite).

SAVING THE POSITIONS OF STANDARDS

1. Locate a standard, right click on the screen, chose 'move to', click 'add', name the position, click set to current stage position and click ok.
2. You may wish to save positions for all standards.
3. If the position of a standard has changed move to the new position, select the standard from the list and click 'edit', then 'update current position'.
4. When you have finished a session and the standards are removed, ensure that you remove (delete) the save positions from the laser software.

RUNNING THE METHOD

The analytical method for laser ablation starts with the user running a number of standards. The first of these standards will be recognized by the '*Glitter*' software and when loaded into a '*Glitter*' processing session will be assigned with a star (*) and data associated with them.
The standards allow the calibration of laser ablation data in two ways:
      -These standards will be used to measure the ablation yield i.e. the amount of material ablated by the laser settings selected.
      -Drift in signal over the period of the analyses and degree of fractionation.
Some standards (internal standards) are run as "unknowns". By analysing material of known composition or age, we can evaluate whether or not our selected standard analyses are valid.

AUTOMATIC ACQUISITION

1. Firstly ICP-MS Top must be configured for automatic acquisition. Close out of ICP-MS Top and open up 'configuration' from the desktop. Under 'remote start' make sure that 'do not use' is not checked. Click save and then reopen ICP-MS Top.
2. A folder on D: drive needs to be created to store your data. If not already created, create a folder. Within this folder is where all your data will be stored, however you should create a new folder within this one for each new sample.
3. On ICP-MS Top edit your sample log table by going to the 'sample' tab and selecting 'edit sample log'. Here you can change the amount of standards you

wish to do between each round of unknowns and change the names of the unknowns.

4. Using the spot creator button on the laser ablation program place spots for the standards to the amount set out on the sample log table of the method being used. Once spots have been made for the standards, move to the 'unknown' sample and place spots on each grain, taking care not to place them on inclusions or over two different growth zones. Make sure that the spot number correlates to the correct sample number in the sample log table, otherwise this will complicate the data interpretation.

5. Once all spots have been placed, acquisition can be started. First select 'start run' in ICP-MS Top. Then click 'run' in the laser ablation program making sure that all spots are selected in the options box that pops up. Click run at the bottom of the box and the laser will track to the first spot and begin the acquisition.

USING GLITTER

1. Open the *Glitter* program from the desktop of the far left computer.
2. Choose 'isotope ratios' when conducting geochronology.
3. To load your data files into glitter, select 'file' > 'load data', and navigate to the I: drive. This is taking the data from the central computer across the network. Then navigate to the root directory of where all your spot analyses are being stored (e.g. D:\username\samplename\), then click ok.
4. A window will then pop up in which the user must set the detector dwell times which have been setup in the method on Chemstation, e.g. for zircon and monazite dating the following dwell times are common and need to be changed in the glitter standards window for each new glitter session. It is critical that the dwell times in the ICP method match those in the glitter standards window.
5. Dwell times for zircon and monazite dating:
   a. Isotope: 204 Dwell time in msec: 10
   b. Isotope: 206 Dwell time in msec: 15
   c. Isotope: 207 Dwell time in msec: 30
   d. Isotope: 208 Dwell time in msec: 10
   e. Isotope: 232 Dwell time in msec: 10
   f. Isotope: 238 Dwell time in msec: 15
6. Click accept, and accept again, and then ok to the next box that pops up.
7. Then choose 'display' > 'age estimates' to display the spot ages.
8. Select 'review signal selection' from the 'window' pull down menu. This window is where you choose to integrate both the background counts, and signal counts from.
9. If conducting standards check that the ages/concentrations match those from the standard block section.
10. After a series of standards have been analysed the glitter program will prompt the user for a different routine for processing the standard/calibration data. To begin with choose 'linear fit to ratios' in the windows options drop down list and then click the close options window. The user may wish to select 'tie standard markers to analyses' in the second drop down list.

EXPORTING DATA

1. Once the required amount of data has been obtained, using the glitter computer select 'file' > 'export'.
2. Leave the default boxes selected, additionally tick 'mean count rates (cps), background subtracted', then click ok.
3. Select the path to save the data to, then click ok.

FINISHING A SESSION AND SHUTTING DOWN THE SYSTEM

1. Select 'instrument' > 'instrument control' in the ICP-MS top program.
2. Turn off the plasma under the 'plasma' drop down menu or hitting the 'plasma off' icon.
3. Turn off the monitors on all three computers. Do not shut down the computers.
4. Shut down the laser ablation software on the right computer. This turns off the light source in the laser unit and saves the bulb.

LA-MC-ICP-MS (Lu-Hf)

Lu-Hf analysis by LA-MC-ICP-MS was undertaken at CSIRO (Waite Campus). Analysis was conducted on the same zircons mounted in epoxy resin used in the U-Pb analysis. The following guide is from Chalk (2014):

Analyses were conducted using a New Wave UP-193 Excimer laser (193 nm) attached to a Thermo-Scientific Neptune Multi Collector ICP-MS equipped with Faraday detectors and $10^{11}\Omega$ amplifiers. The analyses were carried out in a helium atmosphere mixed upstream of the ablation cell with argon and nitrogen. A beam diameter of 50 µm, a 5 Hz repetition rate, and an intensity of approximately 6 J/cm2 were used. Typical ablation times were 60–225 s involving a maximum of 15 measurement cycles, each consisting of ten 0.524 s integrations on ^{171}Yb, ^{173}Yb, ^{175}Lu, ^{176}Hf (+ Lu + Yb), ^{177}Hf, ^{178}Hf, ^{179}Hf and ^{180}Hf; one 0.524 s integration of REE ^{160}Gd, ^{163}Dy, ^{164}Dy, ^{165}Ho, ^{166}Er, ^{167}Er, ^{168}Er, ^{170}Yb and ^{171}Yb, and one 0.524 s integration of Hf oxides with masses ranging from 187 to 196 amu. This is inclusive of a 1.5 s idle time between subsequent mass changes and an off-peak baseline measurement. Oxide formation rates and REE-oxide interference in high REE zircon were monitored throughout the session. No oxide corrections were applied to the data collected during this study. Oxide formation rates were typically 0.02 – 0.03 %. Data were normalised by an exponential mass bias correction using a stable $^{179}Hf/^{177}Hf$ ratio of 0.7325. Isobaric interferences on ^{176}Hf by Yb and Lu were corrected using the methods of Woodhead *et al.* (2004) with direct measurement of $^{171}Yb/^{173}Yb$ fractionation using the Yb isotopic values of Segal *et al.* (2003). Assuming the same mass bias behaviour as Yb, a correction for Lu isobaric interference on ^{176}Hf used a $^{176}Lu/^{175}Lu$ ratio of 0.02655 (Vervoort *et al.* 2004). Data were processed using software *Hf*TRAX v.3.2 (Payne *et al.* 2013). Instrument performance and stability was monitored by analysis of Plesovice ($^{176}Hf/^{177}Hf$ = 0.282482 ± 0.000013, Slama *et al.* 2008) and Mudtank zircon ($^{176}Hf/^{177}Hf$ = 0.282507 ± 0.000006, Woodhead and Hergt 2005) standards. In this study the average $^{176}Hf/^{177}Hf$ values are 0.282470 ± 0.000015 for Plesovice and 0.282506 ± 0.000015 for Mudtank.

XRF Analysis of Major Elements

26 fused discs were made at Mawson Laboratories to be analysed for major elements and trace elements. The following method was used:

1. Wash 26 rimmed glass vials, unrimmed glass vials, plastic caps and ceramic crucibles in warm soapy water, wiping any detritus or labels off using a steel scourer for the vials and caps and a soft cloth for the crucibles.
2. Wash all items in cold tap water to remove detergent.
3. Wash each item three times in RO water.
4. Place the glass vials and ceramic crucibles in an oven, setting temperature to 50^0C. Leave overnight. Air dry plastic caps.
5. Weigh each rimmed vial empty, and also with approximately 4g of sample. Record both these weights. Make sure to label the vial with the sample name contained therein.
6. Leave these samples in an oven overnight at 50^0C again
7. Decant each sample from its vial into a ceramic crucible. Note the number on the crucible and the sample name. Weigh each loaded crucible.
8. Place the crucibles into ceramic trays and place in the furnace.
9. Refer to University of Adelaide XRF disc procedure for instructions on running the furnace
10. Once cycle is completed (approximately 6 hours), take out the trays using oven gloves and place on a cooling block. Leave the samples until the trays are cool enough to hold.
11. Place the sample trays in a desiccator until the samples have cooled to room temperature.
12. Record the new weight of each crucible.
13. For each sample weigh 1g of the sample into an un-rimmed vial and record that weight to 5 decimal places. Then weigh 4g of X-ray flux into the vial and record this weight to 5 decimal places.
14. Close vial with plastic cap and shake liberally in order to make the contents homogeneous.
15. Refer to University of Adelaide XRF disc procedure for instructions on running the XRF disc furnace.

LA-ICP-MS Analysis of Trace Elements

SAMPLE PREPARATION

The XRF discs used for major element analysis can be used for the trace element analysis as outlined by Kil and Jung (2015). The discs were glued together using arts and craft superglue to make a cylinder. Note had to be taken of the order of the discs and the sample numbers of the end discs. Once dry, the cylinder was sawn lengthways in two and one half was stuck to a microscope slide, flat surface down, using epoxy resin. Slide was left to dry for two days. Using a thin section saw, the semi-cylinder was then sliced down so the XRF glass on the microscope slide was only a few millimetres thick. The fresh surface was then polished to remove the saw blade marks and to leave a smooth surface to be ablated by the LA-ICP-MS.

LA-ICP-MS ANALYSIS

Trace Element concentrations were obtained using a New Wave UP-213 laser attached to an Agilent 7500x ICP-MS. The following method from Adelaide Microscopy was used:

Turning on the gases and inserting samples

1. Ensure ICP-MS is in standby mode.
2. Start ICP-MS top program and select the tune menu from the 'instrument' menu.
3. Loosen the screws on the laser ablation chamber door and slide the door to the left. The sample holder will then slide out.
4. Clean your samples and place them in the cell, ensuring they are held tightly.
5. Insert the cell into the chamber, close the door and tighten the screws.
6. Start ICP-MS top program (middle computer).
7. Select 'instrument control' from the instrument menu.
8. Select 'maintenance menu' then 'sample introduction'.
9. Check box 'optional gas' and type 60% for 'optional gas' and click on enter.
10. Open 'laser ablation' program on the New Wave computer (far right computer).
11. Click on 'evacuate' a dialogue box will pop up with a status bar, indicating number of cycles. The laser ablation chamber and then refilled with He in cycles.
12. Once finished click on 'evacuate' twice more. The system needs to do 30 cycles to remove all the air from the chamber.
13. Once finished ensure 'online is selected in the laser ablation program.
14. Close 'sample introduction' dialogue in the ICP-MS top program. This action will reset the optional gas to 0%

Turning on the plasma

1. Select instrument > tune.
2. Select 'optional gas' slider bar (probably set at around 58%) and turn it down to 20%.
3. Select instrument > instrument control.
4. Select instrument > instrument control > start plasma.
5. Wait until the plasma is fully operational (all gauges green, approximately 2 minutes).
6. Go back to instrument > tune and turn optional gas back up to correct value (usually 58-59%).
7. Perform a maintenance log by carrying out the following steps:
    a. On the 'instrument control' screen select the 'diagnostics log' menu and then 'log book'.
    b. Make a note of the 'plasma on' time, then exit.
    c. On the 'Instrument control' screen select the 'maintenance log' menu then 'log book'.
    d. Double click on one of the previous logs, select and copy the information in the 'comments' box. Click close.

      e. Click 'record log' and paste copied data into the 'comments' box, then add in today's details including the 'plasma on' time you made a note of.

      f. Click 'ok' then 'exit'.

8. Select instrument > tune

Load method

1. On the Chemstation computer select the methods menu, load.
2. Select ARTRACE.M for trace element analysis
3. Choose the equivalent calibration file (with a C extension) and click ok.
4. In laser ablation mode (compared to solution ICP-MS) the calibration file is not used however the software will still require this file, if no equivalent calibration file can be found then select Default.C

PA factor

The PA factor allows the ICP-MS software to process signals acquired by the detector in pulse count mode and analogue mode with seamless/linear calibration. This transition in the way the signal is measured occurs when counts per second exceed approximately one million. Thus the PA factor is not required every time the system is run, only when you expect cps to exceed approximately one million in your unknown. When conducting a PA factor what we are attempting to do is trip the detector into analogue counting mode by obtaining over a million counts in at least two elements at opposite ends of the mass spectrum you are analysing. We do this by increasing the spot size and intensity of the laser, and ablate a high concentration NIST glass.

1. Move to Nist 610 (High concentration NIST, dark blue glass).
2. Initially, change the beam to 65 μm and increase frequency to 10Hz.
3. To view the counts on the detector of specific isotopes click on the 'Acq. Params' menu, acquisition parameters, and tick 80, 206, 248/232, 207, 208, 204, 238, 220, click ok. These isotopes will now appear on the tune screen.
4. Start laser firing, click start on the tune screen.
5. When over one million counts in ^{238}U and ^{208}Pb click stop on the tune panel, select tune > P/A factor > click 'load masses from Acq. Method' > run. (Note: If unable to obtain over one million counts, try an 80 μm beam diameter. If sensitivity continues to be too low, try increasing the beam intensity).
6. When the notepad automatically pops up, check that the all the elements are in detection range (they will have a number next to them, usually about 0.9), then click 'yes' to a new P/A factor, click save. (Note: if there are no numbers next to any of the masses, and you did have over a million counts in the tune screen, it could be that you didn't perform step 5 fast enough and the counts dropped below a million. Simply repeat step 5).
7. Stop laser firing, close shutter.
8. Turn the settings back to normal, 5Hz for laser fire rate, 60 μm for spot size and 65% intensity.

Setting up the laser ablation system

1. Open 'laser ablation' program on the New Wave computer.
2. Turn up light intensity and choose COAX mode of sample illumination.
3. Choose 5Hz for laser fire frequency/rate.
4. Select a laser spot size dependent on your method of analysis.
5. Select a power rating. This value is a percentage of the maximum power available, and the value you choose will be dependent on your required spot size and concentration of elements of interest in your sample. Ask an AM staff member if unsure.
6. In order to view the sample surface, the user can adjust the optical zoom. To locate samples use a zero value for the optical zoom, when using the laser increase this zoom to 50%.

Saving the positions of standards

1. Locate a standard, right click on the screen, chose 'move to', click 'add', name the position, click set to current stage position and click ok.
2. You may wish to save positions for all standards.
3. If the position of a standard has changed move to the new position, select the standard from the list and click 'edit', then 'update current position'.
4. When you have finished a session and the standards are removed, ensure that you remove (delete) the save positions from the laser software.

Running the method

The analytical method for laser ablation starts with the user running a number of standards. The first of these standards will be recognized by the '*Glitter*' software and when loaded into a '*Glitter*' processing session will be assigned with a star (*) and data associated with them.
The standards allow the calibration of laser ablation data in two ways:
      -These standards will be used to measure the ablation yield i.e. the amount of material ablated by the laser settings selected.
      -Drift in signal over the period of the analyses and degree of fractionation.
Some standards (internal standards) are run as "unknowns". By analysing material of known composition or age, we can evaluate whether or not our selected standard analyses are valid.

Automatic Acquisition

1. Firstly ICP-MS Top must be configured for automatic acquisition. Close out of ICP-MS Top and open up 'configuration' from the desktop. Under 'remote start' make sure that 'do not use' is not checked. Click save and then reopen ICP-MS Top.

2. A folder on D: drive needs to be created to store your data. If not already created, create a folder. Within this folder is where all your data will be stored, however you should create a new folder within this one for each new sample.

3. On ICP-MS Top edit your sample log table by going to the 'sample' tab and selecting 'edit sample log'. Here you can change the amount of standards you wish to do between each round of unknowns and change the names of the unknowns.

4. Using the spot creator button on the laser ablation program place spots for the standards to the amount set out on the sample log table of the method being used. Once spots have been made for the standards, move to the 'unknown' sample and place spots on each grain, taking care not to place them on inclusions or over two different growth zones. Make sure that the spot number correlates to the correct sample number in the sample log table, otherwise this will complicate the data interpretation.

5. Once all spots have been placed, acquisition can be started. First select 'start run' in ICP-MS Top. Then click 'run' in the laser ablation program making sure that all spots are selected in the options box that pops up. Click run at the bottom of the box and the laser will track to the first spot and begin the acquisition.

Using Glitter

1. Open the *Glitter* program from the desktop of the far left computer.
2. Choose 'element concentration' when conducting geochemistry.
3. To load your data files into glitter, select 'file' > 'load data', and navigate to the I: drive. This is taking the data from the central computer across the network. Then navigate to the root directory of where all your spot analyses are being stored (e.g. D:\username\samplename\), then click ok.
4. A window will then pop up in which the user must set the detector dwell times which have been setup in the method on Chemstation. It is critical that the dwell times in the ICP method match those in the glitter standards window.
5. Click accept, and accept again, and then ok to the next box that pops up.
6. Then choose 'display' > 'age estimates' to display the spot ages.
7. Select 'review signal selection' from the 'window' pull down menu. This window is where you choose to integrate both the background counts, and signal counts from.
8. If conducting standards check that the ages/concentrations match those from the standard block section.
9. After a series of standards have been analysed the glitter program will prompt the user for a different routine for processing the standard/calibration data. To begin with choose 'linear fit to ratios' in the windows options drop down list and then click the close options window. The user may wish to select 'tie standard markers to analyses' in the second drop down list.

Exporting data

1. Once the required amount of data has been obtained, using the glitter computer select 'file' > 'export'.

2. Leave the default boxes selected, additionally tick 'mean count rates (cps), background subtracted', then click ok.
3. Select the path to save the data to, then click ok.

Finishing a session and shutting down the system

1. Select 'instrument' > 'instrument control' in the ICP-MS top program.
2. Turn off the plasma under the 'plasma' drop down menu or hitting the 'plasma off' icon.
3. Turn off the monitors on all three computers. Do not shut down the computers.
4. Shut down the laser ablation software on the right computer. This turns off the light source in the laser unit and saves the bulb.

TIMS Analyses (Sm- Nd, Sr)

5 samples were prepared for TIMS analysis in the following method:

CLEANING THE VIALS

1. Count out the required number of Teflon vials for the analysis based on the number of unknowns and standards required. If you are analysing samples containing zircons or other very hard minerals, 'bombs' will be used in lieu of Teflon vials.
2. All following steps must be undertaken in a fume cupboard.
3. Clean the outside of the vials (and/or bombs) using kimtech wipes and ethanol to remove any previous labels.
4. Partially fill each vial with recycled hydrochloric acid, screw on the lid and leave on a 140^0C hotplate for 30 minutes.
5. Pour the recycled HCl from each vial into a beaker to be decanted into the appropriate waste bottle. Place all the lids and vials into a large beaker of 6M HNO_3.
6. Place a clock glass on top of the beaker concave side up. Fill the clock glass with deionised water to promote condensation of HNO_3 in beaker.
7. Place beaker on hotplate at 170^0C overnight.
8. Turn hotplate up to 500^0C for 10-15 minutes until acid is boiling.
9. Reduce the temperature to 420^0C and leave for 30 minutes.
10. With the aid of silicon mitts, pour away the deionised water in the clock glass, replace the empty glass on top of the beaker. Decant the HNO_3 into another beaker, taking care to keep the vials and lids in the original beaker with the aid of the clock glass.
11. Fill a measuring jug with deionised water and pour contents into the beaker containing the vials, keeping the apparatus in the fume cupboard as fumes can be released when the water is poured into the beaker.
12. Give the beaker a swirl and drain the water away.
13. Repeat steps 11 and 12 two more times to remove any HNO_3 residue.

14. Fill the beaker containing the vials with enough 6M HCl to cover the vials. Place the clock glass back on top of the beaker and fill to the brim with deionised water again.
15. Repeat steps 7 to 13 again (note: acid in this case is now 6M HCl – not 6M HNO_3).
16. Half-fill beaker containing vials with deionised water.
17. Bring beaker to the boil on the hotplate by increasing the temperature to 500^0C.
18. Once the water has reached boiling point, turn off the hotplate. Using the silicon mitts, pour away the water.
19. Shake off any water droplets on the vials and lids.
20. Fill each vial with 1 ml of 6M HNO_3 and 0.5 ml of 6M HF (following HF safety procedures)
21. Screw on the caps and leave on a hotplate at 140^0C overnight.
22. Pour HF:HNO_3 mixture from each vial into a beaker for contents to be evaporated off using a hotplate.
23. Use deionised water to wash away any acid droplets from the Teflon.

PREPARING THE SAMPLE POWDERS

1. The ideal Nd weight for samples is 2 μg. For each 1 μg of Nd, 0.2 g of Sm, Nd spike is required. Therefore each vial needs approximately 0.4g of spike. Use scales for accuracy.
2. Use a static gun to remove the static from the vials.
3. To work out the amount of sample powder needed, an approximate Nd concentration in ppm is required. Divide the concentration by 2 (2 μg of Nd) to calculate the necessary powder weight.
4. Using a spatula, add that amount of powder to the vial.
5. Add approximately 2 mL of HNO_3 to each vial.
6. Add 4 mL of HF to each vial. Leave on a hotplate at 140^0C overnight.
7. Remove caps from vials and leave for 2 hours to allow the contents to go to near-dryness.
8. Top up vials with 1 mL of 15M HNO_3 to stop the samples precipitating as silicon tetrafluorides, which are very insoluble.
9. Once the vials are dry, add another round of 2 mL of 7M HNO_3 and 4 mL of HF and leave to dry.
10. Once again, add 1 mL of 15M HNO_3 and leave to dry.
11. Add 6 mL of 6M HCl to the vials and leave to evaporate off.
12. With the bombs, after adding the second round of HF and HNO_3, they must be placed inside metal bomb jackets and left in an oven at 190^0C for four days.
13. The bomb jackets must be left to cool until they can be handled easily. Open the jackets and remove the bombs.
14. Leave the bombs on a hotplate at 140^0C with the lids off until dry, add 1 mL of 15 HNO_3 and leave to dry.
15. Add 6 mL of 6M HCl and replace back into the oven in the bomb jackets at 150^0C overnight.
16. Remove bombs from jackets and allow them to evaporate to dryness on hotplate.

17. The final steps before mass spectrometer analysis require separating columns to separate the strontium, neodymium and samarium. Refer to the lab notes.
18. Evaporate all the sample vials to dryness on a hotplate.

PREPARING THE FILAMENTS

1. The central filaments are used for Sr, outer filaments Nd and inner filaments for Sm.
2. Using pliers, strip the welded filaments from the towers.
3. Use a hobby grinder to remove any welding left on the towers.
4. Boil the filaments in H_2O_2. Drain and rinse in deionised water three times.
5. Leave filaments in an oven for a few hours to dry them.
6. With clean tantalum strips weld the tantalum to the filament turrets using a welder.

LOADING THE SAMPLES

1. For Sr, insert central filaments onto Centrex filament heater.
2. Pipette 1 µL of 0.5M HNO_3 onto filaments.
3. Turn filament heater up to 0.3A to evaporate off the acid.
4. Pipette 0.5 µL of Sr loading solution.
5. Pipette 1 µL of 1M HNO_3 into sample vial, mix Sr spot with acid.
6. Load 0.5 µL of sample onto a filament and turn heater up to 2A.
7. When sample spot on filament has turned a dull red colour, reduce current to zero quickly.
8. Load filament onto the turret, making note of position number and the sample number.
9. For Nd and Sm, insert outer filaments onto filament heater.
10. Pipette 1 µL of Sm/Nd loading solution onto filaments.
11. Increase current to 0.3A to evaporate solution.
12. Add 1 µL of HNO_3 to sample vials, and mix in the sample spots to dissolve them.
13. Pipette 0.5 µL of sample solution onto filament.
14. Increase current to 1.8A over a period of 20 seconds.
15. Keep at 1.8A for 5 seconds and then take current down to zero.
16. Load filaments onto turret.
17. Run samples in mass spectrometer overnight with guidance of technician.

PROCESSING THE DATA

1. The data will come in spreadsheets. Ask the lab technician for help with which numbers to use and for a spreadsheet to automatically process these numbers.
2. The necessary numbers will be found on the summary sheet of the spreadsheet.
3. Input the numbers into the recommended spreadsheet.
4. All the necessary numbers to construct a εNd diagram will be calculated automatically.

Field Work

From 01/01/2015 to 22/01/2015 field work was carried out in Jebel Ja'alan, near Sur, in the Sultanate of Oman. Using handheld GPS and gridded satellite images and tracing paper, a geological map of the southern flank of Jebel Ja'alan was produced. This highlighted the main lithological boundaries as well as the location of dykes and their dip and dip-direction. 22 rock samples were collected, 5 of the first generation dolerite dykes, 6 of the second generation dolerite dykes, 6 samples of the intermediate dykes, 3 granites, and 2 samples of a mafic intrusion. In addition rock descriptions, field sketches and stereonets were recorded in a notebook to better understand the field relations.

APPENDIX B: RESULTS

Sm-Nd Analysis

Table 3: Results table of Sm-Nd data, including Nd model assumptions and sample measurements.

sample #	dummy	BCR-2	G-2	JA15-14	JA15-18	JA15-25	JA15-34	JA15-42
input age of rock T (Ma)	830	840	840	840	843	840	840	840
Unmixed 143/144Nd	.512979	.512628	.512217	.512965	.512216	.512629	.512615	.512375
Nd ugg^{-1}	24.7	28.8	52.3	11.5	23.7	27.2	37.6	58.8
Sm ugg^{-1}	6.1	6.8	7.9	3.7	4.1	7.3	9.5	14.0
147Sm/144Nd	.1497	.1423	.0916	.1930	.1044	.1616	.1523	.1436
ε Nd (T=0)	6.65	-.19	-8.21	6.39	-8.23	-.17	-.44	-5.14
143Nd/144Nd (T)	.512164	.511844	.511713	.511902	.511639	.511739	.511776	.511584
ε Nd (T)	11.65	5.65	3.09	6.78	1.72	3.59	4.32	.56
TDM (Ma)	403	1102	1156	1310	1291	1499	1309	1663
TCHUR (Ma)	-1116	28	611	-14720	698	39	79	758
DM at age of rock (T)	.511982	.511968	.511968	.511968	.511964	.511968	.511968	.511968
CHUR at age of rock (T)	.511568	.511555	.511555	.511555	.511551	.511555	.511555	.511555

JNdi-1 reference material measured 3/8/12 to 16/8/12, 143/144Nd = .512074 10(sd), 5 measurements.

Nd Model assumptions		
Lambda	6.54E-12	a^{-1}
143Nd/144Nd CHUR T=0	.512638	Goldstein et al (1984)
147Sm/144Nd CHUR T=0	.1966	Goldstein et al (1984)
143Nd/144Nd DM T=0	.513150	Goldstein et al (1984)
147Sm/144Nd DM T=0	.2145	Goldstein et al (1984)
Earth Age	4.615E+09	a

Sample measurements

Sm Nd spike	H rm	H rm	H rm	H rm	H rm	H rm	H rm	H rm
sample wt (g)	.09469	.07847	.05324	.13190	.05568	.13328	.08090	.13412
Sm Nd spike wt (g)	.51115	.46402	.61740	.39971	.39273	.40417	.41006	.39705
measured 143/144Nd	.513036	.512682	.512276	.513034	.512294	.512658	.512650	.512388
2 se (x1E-6)	0	13	25	21	16	27	11	19
measured 150/144 Nd	.496329	.480810	.500019	.548642	.589383	.369192	.396712	.296444
2 se (x1E-6)	0	1972	1881	4633	2348	2026	600	1040
measured 147/149 Sm	4.69050	4.70861	7.71654	4.44090	8.06948	2.75292	3.28540	1.97125
2 se (x1E-5)	0	269	4082	128	838	94	58	243
measured 152/149 Sm	1.89394	1.86102	1.64894	1.90180	1.84474	1.96584	1.90463	1.90754
2 se (x1E-5)	0	1995	1209	658	1028	4290	126	1030

Zircon Lu-Hf Analysis

Table 4: Results table of Lu-Hf analysis, including ratios, epsilon values and model ages.

Sample N	Hf176/Hf177	2 S.E.	Lu176/Hf177	Yb176/Hf177	U/Pb AGE
O1437-04	0.281625989	0.000419	0.00081582	0.025427905	843
O1437-07	0.282505014	5.1186E-05	0.001356775	0.045037183	873
O1437-16	0.306341379	0.03202114	0.0006848	0.050700428	843
O1437-18	0.282431129	0.0001069	0.002678598	0.071287372	830
O1437-20	0.282537935	2.3354E-05	0.000226931	0.008153295	840
O1437-23	0.282482799	5.7744E-05	0.001365396	0.041607486	827
O1437-27	0.282534619	6.4305E-05	0.002343962	0.070299305	855
O1437-44	0.282396539	2.0849E-05	0.000453329	0.010968391	865
JA1533-04	0.282412758	1.9134E-05	0.000351384	0.010616024	900
JA1533-07	0.282430395	3.9002E-05	0.000626659	0.018181022	835
JA1533-08	0.282337784	5.4485E-05	0.001587621	0.049490398	851
JA1533-19	0.282454168	3.0809E-05	0.000567961	0.016935052	787
JA1533-21	0.282425306	2.4144E-05	0.000762043	0.02270304	835
JA1533-24	0.28251756	6.8863E-05	0.002018395	0.055117782	794
JA1533-30	0.282530766	3.422E-05	0.00065876	0.01773555	874
JA1533-31	0.282542034	7.5977E-05	0.002822777	0.067793269	835
JA1533-36	0.282434199	3.3935E-05	0.001634051	0.051819129	853
JA1533-37	0.282401168	4.3822E-05	0.000900173	0.024846312	835
JA1533-38	0.282381	3.4363E-05	0.000459967	0.012934162	805

| Sample N | Scherer et al., 2001 - ^{176}Lu decay constant (1.865x10^{-11}) | | | | |
	Hf$_i$	epsilon	1s	T(DM) (Ga)	T(DM) (crustal)
O1437-04	0.281613	-22.66	14.7	2.27	3.09
O1437-07	0.282483	8.83	1.8	1.07	1.18
O1437-16	0.306331	853.06	1120.7	-50.80	-230.60
O1437-18	0.282389	4.55	3.7	1.22	1.41
O1437-20	0.282534	9.92	0.8	0.99	1.09
O1437-23	0.282462	7.04	2.0	1.10	1.26
O1437-27	0.282497	8.93	2.3	1.05	1.16
O1437-44	0.282389	5.34	0.7	1.19	1.39
JA1533-04	0.282407	6.75	0.7	1.17	1.33
JA1533-07	0.282421	5.77	1.4	1.15	1.34
JA1533-08	0.282312	2.30	1.9	1.31	1.57
JA1533-19	0.282446	5.58	1.1	1.12	1.32
JA1533-21	0.282413	5.52	0.8	1.16	1.36
JA1533-24	0.282487	7.22	2.4	1.07	1.22
JA1533-30	0.282520	10.17	1.2	1.01	1.10
JA1533-31	0.282498	8.51	2.7	1.06	1.17
JA1533-36	0.282408	5.73	1.2	1.18	1.36
JA1533-37	0.282387	4.58	1.5	1.20	1.42
JA1533-38	0.282374	3.45	1.2	1.21	1.46

APPENDIX C: SAMPLES

Table 5: A table of all the samples, their field locations, rock type and undertaken analyses.

Sample Number	UTM Latitude	UTM Longitude	Rock Type	Methods Undertaken
JA15-12	0744781	2451023	Granodiorite	Geochem/zircon
JA15-13	0744781	2451023	Brown Dolerite	Geochem
JA15-14	0744781	2451023	Grey Dolerite	Geochem/Sm-Nd
JA15-16	0744651	2450230	Mafic Enclave	Geochem
JA15-17	0744651	2450230	Grey Dolerite	Geochem
JA15-18	0744651	2450230	Granite	Geochem/zircon/Sm-Nd
JA15-19	0744559	2450332	Andesite	Geochem
JA15-20	0744559	2450332	Grey Dolerite	Geochem
JA15-21	0744559	2450332	Brown Dolerite	Geochem
JA15-22	0744946	2449908	Grey Dolerite	Geochem
JA15-23	0744790	2449849	Brown Dolerite	Geochem
JA15-24	0744758	2449476	Andesite	Geochem
JA15-25	0744822	2449562	Hornblendite	Geochem/Sm-Nd
JA15-30	0743735	2449942	Andesite	Geochem
JA15-31	0743840	2449626	Hornblendite	Geochem
JA15-32	0743552	2449740	Brown Dolerite	Geochem
JA15-33	0743562	2449591	Granite	Geochem/zircon
JA15-34	0743342	2448937	Andesite	Geochem/Sm-Nd
JA15-38	0744439	2459934	Hornblendite	Geochem
JA15-42	0741483	2459356	Brown Dolerite	Geochem/Sm-Nd
JA15-46	0744671	2450248	Andesite	Geochem
JA15-47	0744648	2450240	Andesite	Geochem
JA15-49	0741748	2460439	Brown Dolerite	Geochem
JA15-50	0742489	2448836	Grey Dolerite	Geochem
O14-35	N22 14 00.5	E59 20 38.2	Granite	Geochem/zircon
O14-37	N22 07.699	E59 21.582	Granite	Geochem/zircon